# Characterisation of ozone deposition to a mixed oak-hornbeam forest. Flux measurements at 5 levels above and inside the canopy and their interactions with nitric oxide

Angelo Finco[1], Mhairi Coyle[2], Eiko Nemitz[2], Riccardo Marzuoli[1], Maria Chiesa[1], Benjamin Loubet[3], Silvano Fares[4], Eugenio Diaz-Pines[5], Rainer Gasche[6] and Giacomo Gerosa[1,*]

[1] Dipartimento di Matematica e Fisica, Università Cattolica del S. C., Brescia, Italy

[2] Centre for Ecology & Hydrology, Bush Estate, Penicuik, United Kingdom

[3] Institut National de la Recherche Agronomique, Thiverval-Grignon, France

[4] Council for Agricultural Research and Economics, Research Centre for Forestry and Wood, Arezzo, Italy

[5] Institute of Soil Research, University of Natural Resources and Life Sciences (BOKU); Vienna, Austria.

[6] Institute of Meteorology and Climate Research Atmospheric Environmental Research (IMK-IFU), Garmisch-Partenkirchen, Germany

*Correspondence to*: Giacomo Gerosa (giacomo.gerosa@unicatt.it)

**Abstract**

A one-month field campaign of ozone flux measurements along a 5-levels vertical profile above, inside and below the canopy, was run in a broadleaved mature forest of the Po Valley, Northern Italy. The study aimed at characterizing ozone flux dynamics and their interactions with $NO_x$ fluxes from the forest soil and the atmosphere above the canopy. The ozone fluxes measured at the levels above the canopy were in good agreement among them, thus confirming the validity of the constant flux hypothesis, while below canopy the ozone fluxes were lower than above. However, at the upper canopy edge (24 m) the ozone fluxes were surprisingly higher than above in the morning hours. This was attributed to an ozone sink with NO both emitted from soil and deposited from the atmosphere converging at the top of the canopy. Moreover, this mechanism was eased by the morning coupling between the forest and the atmosphere, while in the afternoon the 24 m fluxes became similar to those of the levels above as a consequence of the in-canopy stratification. Nearly 80% of the ozone deposited to the forest ecosystem was removed by the canopy: 33.3% by the upper canopy layer and 46.3% by the lower canopy layer. Only a minor part of ozone was removed by the understorey vegetation and the soil surface (2%), while the remaining 18.2% was consumed by chemical reaction with soil emitted NO. The collected data could be used to improve the ozone risk assessment for forests and to test the predicting capacity of ozone deposition models, with particular regard to the intra-canopy dynamics of ozone and $NO_x$.

## 1 Introduction

Ozone ($O_3$) had been widely documented as one of the most dangerous pollutant for plants (Wittig et al., 2009; Matyssek et al., 2012; Gerosa et al., 2015; Marzuoli et al., 2018), The deposition of $O_3$ on forest ecosystems has been extensively studied over the last 20 years with eddy covariance field campaigns (Padro, 1996; Cieslik, 1998; Lamaud et al., 2002; Mikkelsen et al., 2004; Gerosa et al., 2005, 2009a, 2009b; Launianen et al., 2013) which were made possible thanks also to the development of fast ozone analysers, functional for such measurements.

Measurements carried out in the 1990´s were usually short-term field campaigns, while more recently campaigns had extended the observation periods and therefore led to a better understanding of the processes controlling ozone deposition (Mikkelsen et al., 2004; Gerosa et al., 2005; Fowler et al., 2009; Rannik et al., 2012; Zona et al., 2014; Fares et al., 2010, 2012, 2014; Clifton et al., 2016, Finco et al., 2017).

These studies highlighted that an important deposition pathway is represented by the ozone uptake by trees, through leaves stomata. The ozone fraction entering the stomata strongly depends on the environmental and physiological factors which drive stomata opening (Jarvis, 1976; Emberson et al., 2000), starting from the soil water availability which is positively correlated to the stomatal ozone flux (Gerosa et al., 2009a; Büker et al., 2012)..

The other ozone deposition pathways are usually grouped as the non-stomatal deposition. The non-stomatal deposition includes many processes which have still to be understood in deep, such as: the thermal decomposition on dry surfaces (Cape, 2009), the deposition on wet surfaces (Fuentes et al., 1992; Altimir et al., 2004, 2006; Gerosa et al., 2009b), reactions stimulated by light (Coe et al., 1995; Fowler et al., 2001), chemical reactions with NO (Dorsey et al., 2004; Rummel et al., 2007; Pilegaard, 2001; Gerosa et al., 2009b), chemical reactions with biogenic, volatile organic compounds (BVOC) (Fares et al., 2010; Goldstein et al., 2004) or the deposition on soil (Stella et al., 2011).

In addition, the ozone deposition below the forest canopy is still unclear. Actually, very few studies have directly measured ozone fluxes below the canopy of the forest, for example, Launianen et al., (2013) and Fares et al., (2014) used these measurements to assess different deposition pathways and to validate ozone deposition models, while Dorsey et al., (2004) focused on the role of soil NO emission in the ozone flux dynamics.

There are still very few studies which reported ozone flux measurements at more than two levels along a vertical profile above and within a forest canopy (Dorsey et al., 2004; Foken et al., 2012), and none of these were made on a mature broadleaf forest according to our knowledge. On the contrary, measurements of vertical gradients of ozone concentration have already been quite investigated (Fontan et al. 1992; Keronen et al. 2003; Utiyama et al. 2003; Gerosa et al. 2005). However, from the latter studies a small to high variability of the ozone concentration inside the canopy emerged and there are still uncertainties on the drivers of these gradients. The major aims of this study were (i) to contribute to the understanding of the diel dynamics of ozone fluxes and ozone concentration gradients at five levels above and within a mature broadleaved forest canopy, (ii) to assess the amount of ozone deposited on the different forest layers (upper canopy, lower canopy, understorey, forest floor), (iii) to evaluate the role of the $NO_x$ exchange on the ozone deposition, both at top canopy and at soil level. In addition, ozone

flux measurements at 5 levels allowed to test the validity of the vertical constant flux hypothesis for this gas in a forest ecosystem.

This work reports data from a joint field campaign which took place in 2012 in the framework of the European FP7 project ECLAIRE ("Effects of Climate Change on Air Pollution Impacts and Response Strategies for European Ecosystems") in the Po Valley (Italy), one of the most polluted areas in Europe. This campaign also included simultaneous flux measurements of volatile organic compounds, particles and ammonia which are reported elsewhere (Acton et al., 2016; Schallhart et al., 2016). The detailed dataset of this campaign will also allow future tests on the capacity of existing deposition models to correctly predict ozone deposition dynamics on forest ecosystems, and particularly intra-canopy dynamics involving ozone reactions with $NO_x$.

## 2 Material and methods

### 2.1 Site characteristics

Measurements were performed at the Bosco Fontana reserve (45°12'02"N, 10°44'44"E; elevation 25 m a.sl.) located in Marmirolo near Mantua, Italy. The measuring site is located just in the middle of the Po Valley, one of the most polluted areas of Europe, and it is represented by a mixed oak-hornbeam mature forest, a typical climax ecosystem for that area, (i.e. an ecosystem at its maximum stage of development). The forest forms part of a 233 ha nature reserve classified as a Site of Communitarian Importance and Special Protection Zone (IT20B0011) and it is part of the Long-Term Environmental Research (LTER) network.

The upper canopy (dominant tree layer) is composed of the higher trees such as hornbeam (*Carpinus betulus*, 40.45 % of the total surface of the reserve), oak (*Quercus robur*, 17.09 %), red oak (*Quercus rubra*, 9.65 %) and Turkey oak (*Quercus cerris*, 7.06 %) (Dalponte et al., 2007). Some species (*Acer campestre*, *Prunus avium*, *Fraxinus ornus and oxycarpa*, *Ulmus minor, and Alnus glutinosa* along the small streams) are present but they account for no more than 3% of the total surface.

The lower canopy (dominated tree layer) is represented by the lower trees and it is composed of hazel (*Corylus avellana*), elder (*Sambucus* spp), cornell (*Cornus mas*), hawthorn (*Crataegus oxyacantha and monogyna*) and chequers (*Sorbus torminalis*). A thick understorey mostly composed of butcher's broom (*Ruscus aculeatus*, L) is also present.

The average height of the canopy is 26 m and the average single-sided leaf area index (LAI), measured by a canopy structure meter (LAI2000), averaged 2.28 $m^2$ $m^{-2}$, with a maximum of 4.22 $m^2$ $m^{-2}$.

The soil is a Petrocalcic Palexeralf, loamy skeletal, mixed, mesic (Campanaro et al., 2007) according to the USDA classification. The soil depth is 1.5 m with petrocalcic hardened layer between 0.80 and 1 m below the ground; this layer was formed after the gradual deepening of the water table.

The climatic characteristics are typical of the Po Valley, with humid and hot summers (Longo, 2004). The mean annual temperature is 13.2°C (period 1840-1997, Bellumé et al., 1998) and July is the hottest month (24.6°C).

The most frequent wind directions are generally from E and NE, in particular in spring and summer.

### 2.2 Measuring infrastructure

A 40 m tall scaffold walk-up tower was built inside the natural reserve (45°11'52.27"N, 10°44'32.27"E), at a distance from the edge of the forest ranging between a minimum of 390 m in the S direction and a maximum of 1440 m in the NE direction.

The infrastructure was equipped with instrumentation for four different kinds of measurements: fluxes of energy and matter ($O_3$, $NO_x$, $CO_2$, $H_2O$) with the eddy covariance technique, soil flux of $O_3$ and $NO_x$ with dynamic chambers, vertical profiles of gas concentrations ($O_3$, $NO_x$) and air temperature and humidity, and additional meteorological and agrometeorological measurements (solar radiation, rainfalls, soil temperature, soil heat fluxes and soil water content).

### 2.3 Eddy covariance measurements of matter and energy fluxes

Four sonic anemometers (see Table S1for instrument models) were placed on the tower at four different heights: 16 m, 24 m, 32 m and 41 m. A fifth one was installed at 5 m a.g.l. on a pole, 10 m away from the tower, in the west direction. At the top tower level an open path infrared gas analyser (Model 7500, LI-Cor, USA) was also installed to measure the concentrations of water vapour and carbon dioxide, and at each of the five sampling heights a fast ozone instrument was installed to measure ozone vertical fluxes.

All the fast ozone instruments (Table S1) were based on the reaction between ozone and a cumarine-47 target which has to be changed after some days because its sensitivity declines exponentially with time (Ermel et al., 2013). Three fast ozone instruments, two COFA (Chemiluminescent Ozone Fast Analyzer) and the ROFI (Rapid Ozone Flux Instrument), which broadly followed the design of the GFAS instrument developed by Güsten and Heinrich, (1996), were equipped with a relatively big fan (about 100 L $min^{-1}$) which resulted in a fast consumption of the coumarin target. The other two instruments, a prototype developed by the National Oceanic and Atmospheric Administration (NOAA, Fast Response Ozone Monitor, Bauer et al., (2000)) and the commercial Fast Ozone Sensor (FOS, Sextant, NZ), both utilized a small membrane pump (2.5 L $min^{-1}$) and thus had a lower consumption of the coumarin targets compared to the other instruments. For this reason, the coumarin targets were changed every 5 days for the COFA and the ROFI and every 10 days for the FROM and the FOS. In both cases the coumarin targets were pre-conditioned just before use by exposing them to a concentration of 100 ppb of ozone for two hours.

Above-canopy fluxes of nitric oxide (NO) were measured at 32 m by means of a CLD780TR fast analyzer (Ecophysics, CH) based on the chemiluminescence reaction between $O_3$ and NO. The air to be analyzed was drawn from 32 m through a 3/8 ID Teflon tube main line at 60 L $min^{-1}$ to the analyzer placed at the bottom of the tower. The analyzer was sub-sampling at 3 L $min^{-1}$ from the main sampling line. The CLD780TR was calibrated with an 80 ppb standard produced using a dilution system (LNI 6000x, S) and a standard NO cylinder (18 ppm), at the beginning of the experiment and then weekly.

All the fast instruments and the sonic anemometers were sampled at 20 Hz through a customized LabVIEW (National Instruments, IRL) program and data were collected and stored in hourly files.

### 2.4 Soil NO, $NO_2$ and $O_3$ flux measurements

Fluxes and concentrations of NO, $NO_2$ and $O_3$ at the soil-atmosphere interface were determined by use of a fully automated measuring system as described in detail elsewhere (Bütterbach-Bahl et al., 1997; Gasche and Papen, 1999; Rosenkranz et al., 2006; Wu et al., 2010). Briefly: five dynamic measurement chambers and one dynamic reference chamber were installed at the site. Dimensions of the chambers were: 0.5 m x 0.5 m x 0.15 m (length x width x height). In contrast to the measuring chambers, the reference chamber was sealed gastight against the soil surface using a plate made of Perspex. Time resolution for flux measurements was 1 hour. Every chamber was closed and measured for 6 minutes, and before every sampling of a measuring chamber the reference chamber was sampled, resulting in a measuring cycle of 60 minutes. During sampling, the air from the chambers was sucked at a constant rate of 50 L $min^{-1}$ and transported via PTFE tubing (inner diameter: 10 mm, length 20 m) to the analyzers. NO and $NO_2$ concentrations were determined using a chemiluminescence detector CLD 770 AL equipped with a photolytic converter (Models CLD 770AL and PLC 760, Ecophysics, CH), and $O_3$ concentrations were determined using an UV ozone analyzer (model TE49C, Thermo Environmental Instruments, USA). Corrections for initial concentrations of NO, $NO_2$ and $O_3$ at the outlet of each chamber and calculation of fluxes of NO and $NO_2$ was performed according to Bütterbach-Bahl et al. (1997). Calibration of the chemiluminescence detector was performed weekly using 40 ppb NO in synthetic air produced by dilution of standard gas (4 ppm NO in $N_2$) with synthetic air (80% $N_2$, 20% $O_2$) using a multi gas calibrator (model 6100, Environics, USA). Efficiency of photolytic conversion of $NO_2$ to NO was determined at least weekly as described in detail by Bütterbach-Bahl et al. (1997).

### 2.5 Vertical profile of $O_3$ and $NO_x$ concentrations and air temperature and humidity

A computer driven system of Teflon tubes and solenoidal Teflon valves was used to characterize the vertical concentration profile of $O_3$ and $NO_x$ above and within the canopy at 6 heights: 5 m, 8 m, 16 m, 24 m, 32 m and 41 m. The air samples drawn through 3/8 ID Teflon tubes (all of them 50 m long) from each level by a 30 L $min^{-1}$ pump were sequentially sent to an UV ozone photometer (model 49C, Thermo Scientific, USA) and to a $NO_x$ chemiluminescence analyser (model 42C, Thermo Environmental Instruments, USA) lodged in an air-conditioned container at the bottom of the tower. Both analyzers were sub-sampling at 2 L $min^{-1}$ out of the 3/8 ID sampling lines.

All the tubes were insulated and continuously purged. Each level was sampled for 4 minutes after 1-minute wait to let the analyzers stabilize and then concentration data were recorded each half an hour with a customized LabVIEW program (National Instruments, USA).

The $O_3$ gradient analyzer was calibrated against a reference photometer before and after the field campaign and no significant deviation from the first calibration was observed. The $NO_x$ analyzer was calibrated with the same procedure described above for the Ecophysics CLD780TR at the beginning of the experiment and then weekly.

Additional $O_3$ and $NO_x$ concentrations at 0.15 m were also available from the soil chambers system previously described.

The ozone concentrations at 5 m, 16 m, 24 m, 32 m and 41 m were also used as absolute ozone reference for the fast ozone instruments all of which change sensitivity sufficiently fast to require constant calibration against a slow response absolute instrument.

Five temperature and relative humidity probes (model HMP45, Vaisala, Finland) were installed, at the higher tower levels (16 m, 24 m, 32 m and 41 m) and, additionally, at 11 m. All these probes were connected to a data logger (CR23x, Campbell Scientific, USA), sampled once per minute and stored as half an hour averages. Two additional temperature measuring points (PT100, Campbell Scientific, USA), were available at 1.5 m and 0.15 m a.g.l. and data were collected with the same personal computer used for the control of the dynamic chamber system.

### 2.6 Additional meteorological and agrometeorological measurements

On the top of the tower a net radiometer NR-lite (Kipp & Zonen, NL), a BF5 sunshine sensor for total and diffuse PAR (Delta-T Devices, UK), a PTB101B barometer (Vaisala, Finland) and a rain gauge (model 52202, Campbell Scientific, USA) were mounted.

Several soil probes were deployed in the soil 20 m from the bottom of the tower: four reflectometers for soil water content (model TDR 616, Campbell Scientific, USA), four soil heat flux plates (model HFP01SC, Hukseflux, NL) and four soil temperature probes (PT100, GMR Strumenti, I). All these sensors were connected to a data logger (CR13x, Campbell Scientific, USA), sampled once per minute and stored as half-hourly averages.

### 2.7 Measuring period

The measuring campaign began on 12$^{th}$ June and ended one month later, on 11$^{th}$ July 2012. From the 12$^{th}$ June to the 23$^{rd}$ June three fast ozone instruments (ROFI, FROM and one of the two COFA samplers) were all placed above the canopy at a height of 32 m in order to compare them and to characterize their performances ("Intercomparison period"). The COFA installed at the top of the tower started its measurements on 12$^{th}$ June and was not moved to level 32 m for the intercomparison because it was already compared with the second COFA before the campaign.

The intercomparison exercise allowed the agreement between the three instruments to be verified, and the average relative standard deviation was below 10%. Considering the intrinsic variation due to the different behaviour of individual coumarin targets no systematic correction was applied. The sextant analyzer, the one employed at 5 m, was calibrated after the field campaign against one of the two COFA. Also in this case, no significant deviation was observed and no corrections were applied.

On 24$^{th}$ June each fast ozone instrument was moved to a different level (Table S1) to begin the flux profile measurements which ended the 11$^{th}$ July ("Flux Profile period"). Every average diel course showed in the following sections is referred to this period.

The FOS installed at 5 m was checked after the field campaign by running it in parallel with the COFA previously used at 32 m in the intercomparison period.

### 2.8 Data processing

The flux measurement technique adopted here was the eddy covariance (Foken, 2008), which states that fluxes are equal to the covariance between the vertical wind component and the scalar of interest (Arya, 2001). An averaging period of 30 minutes was chosen for the calculation of the covariances.

*Despiking*. The data series were divided into 2 minutes sub-series and for each of them block average and standard deviation were calculated. Spikes were identified as the instantaneous data that exceeded the average of each sub-series for more than 3.5 times the standard deviation, as proposed by Vickers and Mahrt (1997). Spikes were removed from the series and the data were then gap-filled by a linear interpolation.

*Rotations*. Two axis rotations were applied to the instantaneous wind components to align $u$ with the mean flow over the averaging period: the first rotation aligned the horizontal wind to the 30 minutes average $u$ component (this rotation forces $\bar{v} = 0$), and the second one to rotate the *xy* plane in order to zero the 30 minutes average vertical component of the wind ($\overline{w} = 0$) (McMillen, 1988; Wilczak et al., 2001). These rotations corrected the little imperfections in the vertical alignment of the sonic anemometers and prepare the data for flux calculations. Samples with a second rotation (vertical tilt) angle greater than 15° were discarded.

*Linear detrending*. The fluctuations of each parameter (w', T', $O_3$') were calculated as the differences of each instantaneous value from the best linear fit (minimum square) of the considered time series in each half an hour data (Lee at al., 2004).

*Time-lag determination*. Ozone fluxes were calculated using a fixed time-lag between the vertical wind time series and the ozone concentration one. For each fast instrument the time lag which maximized the cross-covariance function between the vertical component of the wind and the ozone concentrations was identified and the more frequent lag was used in the calculations for every half an hour.

*Elimination of the kinematic fluxes below the error threshold*. The error threshold was quantified for each half-hourly data series by following the methodology proposed by Langford et al., (2015). The standard deviation of the auto-correlation function was calculated for each half-hourly data chunk, with lags ranging between 30 and 60 seconds from the characteristic time lag of each instrument. Kinematic fluxes lower than three times the standard deviation (relating to the 95$^{th}$ percentile) of were discarded.

*Frequency loss correction.*

The frequency loss correction factors for the different fast ozone analyzers were calculated using the experimental transfer function approach following the methodology proposed by Aubinet et al. (2000). This method considers the normalized cospectra for sensible heat as unaffected by frequency loss or, at most, affected by frequency loss which are negligible respect to those related to the other considered. The transfer function is calculated for every half-hour as the ratio between the normalized cospectra of ozone (in our case) and the normalized cospectra of sensible heat, then fitted with a Gaussian type function (Aubinet et al., 2001), and thus used to calculate a correction factor for each instrument. For further details, please refer to Aubinet et al. (2012).

*Schotanus and WPL corrections*. Fluxes of sensible heat (H), latent heat (LE) and trace gases were corrected for air density fluctuations. The formulation adopted for the correction of H was the one proposed by Schotanus et al., (1983) while the formulation used for LE and trace gases was the one proposed by Webb et al., (1980).

*Calculation of fluxes in physical units.* Fast ozone concentration data –acquired as voltages- and fast NO concentration data – acquired as counts per seconds- required additional processing to calculate quantitative fluxes in physical units. First, for all the fast ozone instruments the target zero $V_0$ (Muller et al., 2010) – i.e. the output voltage when ozone concentration is 0 ppb – was identified for each coumarin target employed. Then the ozone fluxes were calculated by the following equation (Muller et al., 2010):

$$F_{O3} = \frac{\overline{w'V'}}{\bar{V} - V_0} C_{O3} \quad (1)$$

where $\overline{w'V'}$ is the covariance between the vertical wind component and the raw output voltage of the fast ozone instrument, $\bar{V}$ is the average output voltage of the instrument in each half an hour, $V_0$ is the zero target, identified for the considered half an hour, and it represents an estimation of the voltage at zero ozone concentration, and $C_{O3}$ is the ozone concentration measured by the reference ozone analyzer averaged over the same period. The data of the two hours following each target change were excluded in order to allow the target sensitivity to stabilize after the target installation.

Similarly, NO fluxes were calculated using the following equation:

$$F_{NO} = \frac{\overline{w'cps'}}{\overline{cps} - cps_0} S_{NO} \quad (2)$$

where $\overline{cps}$ (counts per seconds) is the NO raw data measurement averaged in each half an hour, and $cps_0$ and $S_{NO}$ are the offset and the sensitivity of the analyser determined by calibration. $Cps_0$ ranged from 1000 to 2500 cps while $S_{NO}$ ranged from 10000 to 12000 cps / (µmol $m^{-3}$).

*Ozone storage*. Ozone fluxes measured by eddy covariance were corrected for the ozone storage every half-hour. The ozone storage is the temporal variation of the vertical ozone profile below the measuring point located at the height $z_m$. It does not represent a true ozone removal or production process, but only a temporary accumulation of ozone in the air column below the measuring point or a temporary ozone release out of the same air column. For a non-reactive tracer, the proof of it is that the storage integrated over a whole day is null. The calculation of the ozone storage is necessary for a proper determination of the ozone deposition processes.

The correction of the ozone fluxes for the storage was made by means of the following equation (Rummel et al., 2007):

$$F_{StorO_3} = F_{O_3} + \frac{\partial}{\partial t} \int_0^{z_m} O_3(z) dz \quad (3)$$

where $F_{StorO_3}$ are the ozone fluxes corrected by storage, $F_{O_3}$ are the measured ozone fluxes obtained with the Eq. (1), and the second term on the right represents the ozone storage term. For a reactive tracer like ozone some of the stored gas may be destroyed by reaction with NO and potentially with VOCs before being re-released to the air space above, and thus, Eq. (3)

must be considered an approximation. A fully resolving 1D chemistry and exchange model would be required to quantify the effect of chemistry on the storage term more fully.

*Stationarity check.* Finally, the stationarity of each half-hour sample was verified following the methodology of Foken and Wichura (1996) and the non-stationary data were discarded.

## 3 Results

### 3.1 Microclimate

Significant rainfalls had cooled the air before the beginning of the field campaign so that, air temperature increased significantly in the first days and after that remained stable (Figure S1a). The average temperature at the top of the tower was 25.9 °C, while the lowest average temperature (23.1 °C) was recorded at 0.15 m. The maximum temperature during the whole period was 36.2 °C which was observed at the top of the canopy (24 m).

On average the temperature minimum was observed during night around 3:00 (solar local time, always the same hereafter) (Figure 1b) for the levels from 11 m to 24 m and one hour later for all the other levels, with values ranging from 19 °C to 21 °C. Two significant rainfall events occurred in the final part of the campaign accounting for a total of 108 mm of rain, but these did not affect significantly the air temperature (Figure 1a). In general, most of the days were sunny (only three days were partially cloudy) and humid, with nighttime peaks of relative humidity up to 80% and diurnal minima around 40%. Specific humidity $q$ ranged, on average, between 10 and 13 $g_{H_2O}/kg_{air}$ (Figure 1a). Below canopy levels (≤ 16 m) showed higher $q$ than the above canopy levels early in the morning, around 6:00, and from 13:00 to 21:00, while the top-crown level (24 m) showed the lowest $q$ values from 4:00 to 16:00. Specific humidity showed close agreement amongst the above canopy levels, with slightly higher values at 41 m.

The wind blew mostly from the East or West, with about 50% of the data in these directions (Figure 1c), whilst the N and S directions accounted for 12% of the data and the intermediate directions accounted for less than 20% of the data. The diurnal wind intensity at 41 and 32 m was on average around 2 and 1.5 m $s^{-1}$ respectively (Figure S1d), and the wind intensity was slightly greater during night than during daytime, with nearly 1 m $s^{-1}$ more at 41 m and 0.5 m $s^{-1}$ at 32 m. The three lower levels showed very low intensity, below 0.5 m $s^{-1}$, with only a minor increase during the day.

The friction velocity ($u^*$) at the two upper levels above the canopy showed a very similar behaviour (Figure 1b) but $u_*$ was slightly higher at 32 m (+6%). Diel maxima of $u_*$ were about 0.5 m $s^{-1}$ occurring between 9:00 and 13:00, after which they suddenly decrease of nearly 20% and then gradually decreased. The minimum (0.13 m $s^{-1}$) was observed around 20:00, after that a quite irregular behaviour during the night was observed with values between 0.2 and 0.3 m $s^{-1}$. The in-canopy measurements of friction velocity at the lowest three levels were significantly lower than the above canopy ones: 24 m and 5 m measurements were less than 50% of the two upper levels and 16 m measurements were around 70% less than above canopy levels. The diurnal maxima at noon were 0.25 m $s^{-1}$ at 24 m, 0.18 m $s^{-1}$ at 16 m and 0.26 m $s^{-1}$ at 5 m and during the night the

friction velocity showed a flatter trend with values below around 0.1 m $s^{-1}$ at 5 m and around 0.05 m $s^{-1}$ for the two others levels.

### 3.2 Profiles of temperature, heat fluxes and atmospheric stability

Following sunrise, early in the morning, the heating of the top part of the canopy developed a thermal inversion in the forest with the ceiling at the top of the canopy (level 24 m) and the base at ground level (Figure 2a).

Above the canopy temperature gradients were strongly super-adiabatic from 4:00 to 17:00, however it should be noted that heat transfer increased significantly only when friction velocity increased.

During the morning, the gradual heating of the canopy extended to the upper canopy layer, reaching its maximum value at noon. As a consequence, the inversion ceiling was lowered to the bottom part of the tree crowns (16 m). But already from 2 pm the air layers in the middle of the trunk space started to cool and the inversion ceiling gradually reached the top of the canopy. By 6 pm the top of the canopy had cooled sufficiently for and the above-canopy atmosphere to become stable, which then attenuated overnight, without ever disappearing (Figure 2b).

The presence of an inside canopy thermal inversion is confirmed also by the measured sensible heat fluxes (Figure 3). Above the canopy the heat fluxes were strongly upward during the day. However, the sensible heat fluxes at 32 m were about 20% larger than those at 41 m.

In the upper part of the crown (24 m), sensible heat fluxes were less than half the above canopy ones in the central part of the day. On the contrary, the heat fluxes at 16 m and 5 m were almost always zero or negative (directed downwards). In relation to the strengthening of the thermal inversion in the afternoon, it is worth noting that the downward heat fluxes peaked at 2 PM at 5 m, two hours later at 16 m and four hours later at 24 m.

However, the forest released most of the energy as latent heat with a peak around 300 W $m^{-2}$ at midday and with very small nighttime values.

Above the canopy the atmosphere was nearly always unstable during the day, while below canopy it was mostly stable, as shown in Figure 4. At the top canopy level (24 m) the most frequent condition in the central hours of the day was strong instability because of the canopy heating due to the radiation. Remarkably, stable conditions at this level strengthened from 3 pm to 7 pm just during the inversion.

Inside the canopy (16 m) the atmosphere was mainly stable or very stable. In particular, from 14:00 to 19:00 the inside canopy air was almost always very stable, as it happened for a shorter period in the morning from 6:00 to 8:00. During the night the atmosphere was mainly stable or very stable above canopy, while at 24 m and 16 m some nocturnal instability was observed, this latter might be due to numerical artifacts because the sensible heat fluxes were close to zero. A similar explanation can be used also for the stability class distribution at 5 m, for which some instability was observed. In any case, stable condition was the most frequent situation observed at that level.

### 3.3 Ozone concentrations profiles

Ozone concentrations above the canopy (41 m and 32 m) showed the typical bell-shaped diurnal pattern, with a maximum around 80 ppb at 14:00 and minimum around 25 ppb at 4:00 (Figure 5). The concentrations decreased slightly throughout the canopy (-9% between 32 m and 5 m), while there was a significant reduction near the ground (-72% between 32 m and 0.15 m). At ground level, average ozone concentrations never exceeded 27 ppb. It is worth noticing the second (relative) minimum observed at 16:00 at the lowest level; this minimum is in agreement with a slight reduction in the ozone concentrations observed in the upper levels inside the canopy (from 5 m to 24 m). These features can be better observed considering the vertical variations in Figure 6a and Figure 6b. During the night the in-canopy gradient of ozone was negligible, but from early morning a negative gradient rapidly developed and remained almost constant (around 0.2 ppb $m^{-1}$) during the daylight hours, except in the afternoon. The slope of this gradient increased in the afternoon: at 16:00 from 8 m to 32 m (around 0.5 ppb $m^{-1}$) and at 18:00 but only from 24 m to 32 m (around 0.8 ppb $m^{-1}$). Another peculiarity emerged from 13:00 to 15:30, when the ozone concentration just above the canopy (32 m) was on average higher (by 2.0 to 3.8 ppb) than above (41 m); moreover, in the same period, also the 24 m ozone concentration was higher than the one measured at 41 m (from 1.2 to 2.5 ppb).

### 3.4 Ozone fluxes profile

Ozone fluxes were corrected for the storage in the air layers below each measuring point. The magnitude of these corrections was not negligible and they were higher in the morning and in the evening (Figure S2) when the air layers in the trunk space are respectively refilling and emptying of ozone. Considering the whole 41m height air column, the greatest storage correction was nearly +5 nmol $m^{-2}$ $s^{-1}$ in the morning, while in the evening it was about -4 nmol $m^{-2}$ $s^{-1}$, the integrated value over the day was null.

Ozone fluxes showed a regular behaviour with almost always negative values except for some positive peaks during night or during the transition between night and day, in particular in the lowest levels (Figure 7). The largest deposition flux was observed on 25$^{th}$ June at the 24 m with 46 nmol $m^{-2}$ $s^{-1}$ level in agreement with a peak of evapotranspiration (Figure S3). The following two days were nearly 50% lower and LE fluxes too. In general, ozone fluxes and LE fluxes seem to be correlated but there were some exceptions for instance on 3$^{rd}$ and 4$^{th}$ July. The smallest fluxes were observed on 6$^{th}$ July during the rainfall events, after which the ozone fluxes showed an increase (7$^{th}$ July) even if ozone concentrations were lower, corresponding to an increase of soil water content and evapotranspiration fluxes.

The diel average course of ozone fluxes (Figure 8) showed at all the levels the typical behaviour with low nighttime values and the greatest deposition in the central hours of the day.

Ozone fluxes measured above the canopy (41 m and 32 m) showed very good agreement, nearly overlapped during the day (Figure 8). Both increased very rapidly in the morning and then stayed almost constant (between 8 and 10 nmol $m^{-2}$ $s^{-1}$) from 9:00 to 16:00, when they started to decrease. At 24 m, fluxes were not constant in the central part of the day and they were on average 40% greater than the above canopy levels with average peaks around 15 nmol $m^{-2}$ $s^{-1}$ (Figure 8). From 9:00 to 16:00,

air layers above canopy including the top of the crown (from 24 m to the top of the tower), seemed decoupled from the air below: the above layers were in superadiabatic conditions with intense air mixing (Figure 4a and 4b) while the below canopy experienced a thermal inversion which gradually expands towards the top of the canopy and even above after 16:00 (Figure 2b).

Greater fluxes at 24 m might be caused by the location of these measurements which are just in the transient region between well mixed superadiabatic air and the below canopy thermal inversion.

### 3.5 NO and $NO_2$ fluxes and concentrations

NO and $NO_2$ concentrations along the tower profile (excluding near ground measurements at 0.15 m) were relatively low with a maximum early in the morning respectively around 2 ppb for NO and around 14 ppb for $NO_2$. Both NO and $NO_2$ concentrations did not show great differences along the vertical profile (Figure 9a and Figure 9b). The greatest differences between the bottom and top level were only around 1 ppb, for both compounds, very early in the morning, between 4:00 and 9:00.

At soil level (0.15 m) the behaviour was completely different for both compounds. NO was always greater than the above levels (from 5 m to 41 m) with two peaks (Figure 9b): the first one at 6:00 around 15 ppb and the second one in the afternoon around 17:00 (nearly 20 ppb). $NO_2$ at soil level was relatively constant ranging from 7 to 12 ppb; even in this case two peaks were observed: at 6:00 (10 ppb) and around 17 (11 ppb).

NO and $NO_2$ fluxes at ground level were almost always mono-directional with NO emitted from soil and $NO_2$ deposited to the ground (Figure 9c). A significant change in the emission rate of NO and in the deposition of $NO_2$ was observed after the rainfalls happened between 6$^{th}$ and 7$^{th}$ July (Figure 9d).

The average diel course of soil fluxes showed an almost constant emission of NO with two decreases: the first one around 6:00 and the second one at 17:00. These two decreases of the observed fluxes were strictly linked with the stratification of the air above ground: an increase in the concentrations in a stratified environment led to a reduction of the concentration gradient between soil/litter and the atmosphere thus reducing the emission in turn. The average diel course of $NO_2$ deposition were nearly inversely proportional to the behaviour of the NO soil fluxes with a pronounced reduction of the deposition early in the morning and a less intense one in the afternoon. In the afternoon, the nearly simultaneous minimum of soil NO fluxes and maximum of $NO_2$ deposition (Figure 9e) indicates a gas phase titration with an ozone reduction by NO (Figure 5).

At the top canopy the net exchange of NO with the above atmosphere was very small except in the morning (Figure 9e), when the deposition peak between 6:00 and 11:00 reached -15 µg N $m^{-2}$ $s^{-1}$. This NO deposition (Figure 9e) is correlated to the development of a small NO gradient above the canopy (Figure 9b) after the $NO_2$ photolysis. The NO gradient and fluxes became negligible (Figure 9b and Figure 9e) when $NO_2$ concentrations reached a minimum (Figure 9a) determined by the photolytic equilibrium of $NO_x$.

**4 Discussion**

Whilst turbulence and heat fluxes inside tree canopies had been studied more extensively, only few studies had attempted to partition ozone fluxes by means of flux measurements at different in-canopy heights (Dorsey et al., 2004; Launiainen et al., 2013).

The evaluation of flux profiles relies on the constant flux hypothesis, one of the most fundamental theories of micrometeorology (Arya, 1989). In the case of the Bosco Fontana measurements, one would expect that the fluxes measured at 41 m and at 32 m should be almost equal and then the deposition flux should decrease, in absolute terms, at the lower levels due the presence of different in-canopy sinks for momentum and ozone (stomata and surfaces of the leaves, branches and stems), and sinks and sources for heat. Consistent with this expectation, measured fluxes of heat and momentum were significantly reduced within the canopy. This may be due to differences in the flux footprint, coupled with heterogeneity in the canopy (Dalponte et al., 2007; Acton et al., 2016), but it does not appear to be dependent on wind direction. Because the 32 m measurements were made lower within the surface roughness layer, it is possible that fluxes were locally somewhat enhanced. Fluxes of ozone were similar at these two above-canopy heights, within the uncertainty of the measurement, but unlike for the fluxes of heat and momentum, measurements at 24 m showed a significantly larger ozone deposition than the two upper levels (32 m and 41 m) at certain times of the day. In the morning (9:00 to 12:00) 24 m ozone fluxes were on average nearly 3 nmol $m^{-2}$ $s^{-1}$ larger than above the canopy (Figure 8), while they were nearly equal on average from 13:00 to 18:00 (fluxes at 24 m were only 0.5 nmol $m^{-2}$ $s^{-1}$ larger).

A possible explanation of these differences could lie in the different footprints of the eddy covariance measurements. The footprints of the measurements at 41 m, 32 m and 24 m were all falling inside the surface of the upper forest canopy, even though the 24 m level was just at the top canopy edge. The size of the footprint areas obviously decreased at decreasing measuring heights. However, in absence of any source or sink of the considered scalar, the horizontal homogeneity of the studied ecosystem ensures the validity of the constant flux hypothesis and thus the measurements referred to different footprints should be the same, i.e. fluxes with larger footprints (measurements at 41 m and 32 m) should be comparable to those with smaller footprints (measurements at 24 m). In order to investigate alternative reasons for the enhancement of the ozone fluxes at 24 m a spectral analysis was performed to compare the normalized cospectra of the ozone fluxes at the different levels, and the role of the NO-realated ozone chemical sink was analysed.

Figure S4 shows the average normalized cospectra of the vertical component of wind and ozone for the measurements performed when the morning ozone enhancement at 24 m occurred (11:00) and when the 24 m ozone fluxes were comparable with the upper ones (15:00).

The cospectra analysis did not provide an obvious explanation for the enhancement of the fluxes observed at 24 m in the morning. Apart from the ozone cospectra at 16 m which had a very irregular behaviour, the other three cospectra did not show any particular difference which could explain the higher ozone fluxes at 24 m. The observed decrease of the ozone cospectra

at 24 m and 16m for frequency above 0.1 Hz is consistent with the notion that within the canopy the mean eddy-size is dictated by the canopy height.

The analysis of the NO related chemical sink instead, revealed a possible role of the convergence of two NO fluxes at the top of the canopy on the enhancement of the O3 fluxes at 24 m, i.e. the NO deposition flux from the air above the forest and the soil NO emission flux uprising from the forest floor. This can be argued by considering the differences between the $O_3$ fluxes measured at 24 m and those measured at 32 m (a level where the constant flux hypothesis is confirmed). The sum of these differences from 6:00 to 12:00 in the morning gives a value of 59.4 μmol $O_3$ $m^{-2}$, which is almost equal to the sum of the NO converging to the top of the crown both from above and below the canopy in the same hours (54 μmol NO $m^{-2}$).

Supposing a stoichiometric reaction between NO and $O_3$ at the top of the canopy, by subtracting to the 24m O3 fluxes an amount of ozone equal to the NO converging at the top of canopy every half-hour, the part of the $O_3$ flux not caused by this chemical sink is obtained. This is shown in the Figure 10 where the measured $O_3$ flux at 24 m is represented as a green line and the resulting part of the $O_3$ flux at 24 m not due to the NO sink is reported as a dark grey dashed line, being the NO fluxes converging from above and below canopy represented by the black and purple lines respectively.

The good agreement between the ozone fluxes at 32 m (Figure 10, red line) and the part of the $O_3$ flux at 24 m not due to the NO sink (Figure 10, dark grey dashed line) suggests that the enhancement of the $O_3$ fluxes observed at 24 m was related to the interactions of $O_3$ with NO at the top canopy level. The contribution of the NO emitted by soil to the observed ozone flux was relatively constant and greater than the contribution of the NO transported into the forest from the atmosphere above, because this latter was very low in the afternoon and relatively high only in the morning (Figure 9e). This observation is supported by the increased ozone fluxes at 24 m which were observed mostly in the morning and nearly ceased in the afternoon.

A possible explanation could be found in the forest-atmosphere decoupling during the afternoon compared to the forest-atmosphere coupling observed in the morning. In fact, the increase of the NO concentrations at soil level (0.15 m, Figure 9b) after midday, followed by the decrease of $O_3$ concentrations at the same level (Figure 5), suggests an air stratification inside the canopy and its decoupling from the above canopy air, as also found by Rummel et al., (2002) and Foken (2008). On the contrary the decrease of the soil level NO concentration (Figure 9b) from 6:00 to 12:00 in the morning suggests a relatively well-mixed canopy which is better coupled with the atmosphere above. This condition allowed also ozone and NO from the above canopy air to penetrate more easily into the canopy (see Figure 6b and the morning peak of Figure 9b). The afternoon stratification is also supported by the stability classes reported in Figure 4c and Figure 4d which were almost always stable or very stable both at 16 m and at 24 m from 15:00 to 18:00. In addition, the thermal inversion layer within the canopy increased its thickness during the afternoon (Figure 2b) rising form the 16 m observed around 12:00 to the 24 m observed from 14:00 to 16:00. Again, the morning coupling and the afternoon decoupling is supported by the diurnal course of the specific humidity observed below canopy (Figure 1a). In the morning the almost constant amount of water vapour above and below canopy (a part from the top-canopy 24 m level where there was an unidentified process removing water vapour) reveals an efficient mixing of the air while in the afternoon the increase of the specific humidity from the three lower levels, due to soil evaporation and understorey transpiration, reveals an air stratification below canopy and a forest decoupling from the above atmosphere.

The availability of ozone flux measurements at different heights within and above the canopy allowed a partition of the ozone fluxes among the different ecosystem layers: upper and lower crown, understorey and soil. To do that we have assumed the ozone flux measured at 32 m as a total deposition flux, then we calculated the NO sink as the sum of NO deposited from the top and emitted from soil assuming a stoichiometric reaction between NO and $O_3$. The ozone taken up by the upper canopy layer was identified as the difference between the ozone fluxes measured at 32 m and those measured at 16 m (ignoring the apparently enhanced values at 24 m), while the ozone taken up by the lower canopy layer was obtained as the difference between the ozone fluxes measured at 16 m and 5 m. Finally, the deposition to the forest floor (soil and the understorey vegetation) was calculated as the difference between the ozone flux at 5 m and the NO flux emitted by soil, namely the amount of ozone which is not removed by chemical reaction with NO.

The result of this exercise is shown in Figure 11, where it can be observed that the upper canopy layer of the forest removed about 1/3 of the total deposited ozone while the lower canopy layer of the forest removed the main part of the ozone (46.5%). The canopy removed nearly 80% of the ozone deposited to the forest ecosystem, but it is worth noticing that this amount includes both stomatal and non-stomatal uptake.

Only a minor part of $O_3$ was removed by the understorey vegetation or deposited to the soil (2.0%) while an important role was played by the NO sink, mainly due to soil emissions, which accounted for the 18.2% of the total ozone deposition.

This latter result is in general agreement with the observations of Dorsey et al., (2004) who found that in a Douglas fir plantation between 7% and 14% of the ozone deposition in the daylight hours could be attributed to the reaction with the soil emitted NO, while this fraction increased up to 41% during the night. Similarly, Pilegaard (2001) found that the NO sink accounted for a 25% of the ozone deposition in a Norway spruce forest, with an increase of this fraction up to 31% during the night.

Nearly all the nighttime ozone deposition at Bosco Fontana can be attributed to the NO depletion of ozone, which resulted the responsible process for the observed ozone deposition at night. The fact that NO reaction accounts for 100% of the nocturnal $O_3$ deposition would imply that other non-stomatal sinks are negligible during that time. It cannot have completely ruled out, however, that our stirred soil flux chambers could somewhat overestimate the nocturnal soil NO emission, due to the enhanced amount of mixing in the flux chamber compared with the true forest floor during calm nights. Similarly, the analysis assumes that the only sink of NO is reaction with $O_3$. A small amount of uptake of NO by vegetation is possible even if unlikely as shown by Teklemariam et al., (2006) and Stella et al. (2013). Overall this ecosystem did not behave as a net NO emitter because the whole NO produced at soil level is consumed within the canopy, but as a weak NO sink because of the small amount of NO received from the atmosphere in the first hours of the morning (Figure 9d). This differs from the observation of Dorsey et al. (2004) who estimated that nearly 60% of the NO emitted from the soil of a Douglas Fir forest escaped the trunk space to react aloft.

## 5 Conclusions

Ozone flux measurements were run along a vertical profile with five measuring points above, inside and below the canopy. The ozone flux measurements of the levels above the canopy were in good agreement between them and comparable with values reported for other forest types (Amthor et al., 1994; Gerosa et al., 2005, 2009a; Fares et al., 2014; Finco et al., 2017), since no measurements on oak-hornbeam forests were found in the literature. Ozone fluxes at 16 m and 5 m were lower than above the canopy, while at the top canopy edge (24 m) fluxes were surprisingly higher than above in the morning hours. The main cause of this enhancement has been attributed to an ozone sink due to a reaction with NO both emitted from soil and deposited from the atmosphere above the canopy. The morning enhancement of the ozone fluxes at 24 m was eased by the coupling between the forest and the atmosphere, while in the afternoon the decoupling and the in-canopy stratification led to 24 m fluxes comparable to those above the canopy.

Most of the ozone, nearly 80%, was removed by the forest canopy: in particular, the upper canopy layer removed 33.3% of the ozone deposited and the lower canopy layer 46.3%. Only a minor part of ozone was deposited on the soil and the understorey (2%), while the remaining part (18.2%) was removed by a chemical reaction with NO emitted by the soil. These findings might be useful to improve the ozone risk assessment for mature forests.

Finally, the complex diel dynamics of ozone and NOx observed at Bosco Fontana represent a challenge for modelists. The collected data will be available for the parameterization and the fine tuning of process models aimed at correctly reproducing the intra-canopy dynamics of ozone and $NO_x$

*Acknowledgements.* The authors are grateful to the administration and the personnel of the Bosco Fontana National Reserve for their availability and continuous support, to the European Union for having fund the project ECLAIRE under which this campaign was made.

This publication was funded by the Catholic University of the Sacred Heart in the frame of its Programs of promotion and dissemination of the scientific research.

**References**


- Acton, W. J. F., Schallhart, S., Langford, B., Valach, A., Rantala, P., Fares, S., Carriero, G., Tillmann, R., Tomlinson, S. J., Dragosits, U., Gianelle, D., Hewitt, C. N., and Nemitz, E.: Canopyscale flux measurements and bottom-up emission estimates of volatile organic compounds from a mixed oak and hornbeam forest in northern Italy, Atmos. Chem. Phys., 16, 7149–7170, doi:10.5194/acp-16-7149-2016, 2016.
- Altimir, N., Tuovinen, J.-P., Vesala, T., Kulmala, M., and Hari, P.: Measurements of ozone removal to Scots pine shoots: calibration of a stomatal uptake model including the non-stomatal component, Atmos. Environ., 38, 2387–2398, 2004.
- Altimir, N., Kolari, P., Tuovinen, J.-P., Vesala, T., Back, J., Suni, T., Kulmala, M., and Hari, P.: Foliage surface ozone deposition: a role for surface moisture?, Biogeosciences, 3, 209-228, doi: http://www.biogeosciences.net/3/209/2006/, 2006.
- Arya, S. P.: Introduction to Micrometeorology, Academic Press, San Diego, USA, pp 415, 2001.
- Amthor, J. S., Goulden, M. L., Munger, J. W., and Wofsy, S.C.: Testing a mechanistic model of forest-canopy mass and energy exchange using eddy correlation: carbon dioxide and ozone uptake by a mixed oak-maple stand, Func. Plant Biol., 21, 623-651, 1994.
- Aubinet, M., Grelle, A., Ibrom, A., Rannik, U., Moncrieff, J., Foken, T., Kowalski, A. S., Martin, P. H., Berbigier, P., Bernhofer, C., Clement, R., Elbers, J., Granier, A., Grunwald, T., Morgenstern, K., Pilegaard, K., Rebmann, C., Snijders, W., Valentini, R., and Vesala, T.: Estimates of the annual net carbon and water exchange of forests: The EUROFLUX methodology, Adv. Ecol. Res., 30, 113–175, 2000.
- Aubinet, M., Chermanne, B., Vandenhaute, M., Longdoz, B., Yernaux, M. and Laitat, E.: Long term carbon dioxide exchange above a mixed forest in the Belgian Ardennes, Agric. For. Meteorol, 108, 293–315, 2001.
- Aubinet, M., Vesala, T., Papale, D. (Eds): Eddy Covariance. A practical guide to measurement and data analysis. Springer, Netherlands, 2012.
- Bauer, M. R., Hultman, N. E., Panek, J. A., and Goldstein, A. H.: Ozone deposition to a ponderosa pine plantation in the Sierra Nevada Mountains (CA): A comparison of two different climatic years, J. Geophys. Res.- Atmos., 105, 22123–22136, 2000.
- Bellumè M., Maugeri M., and Mazzucchelli E.: Due secoli di osservazioni meteorologiche a Mantova, Edizioni CUSL, Milano (Italy), pp. 124, 1998.
- Büker, P., Morrissey, T., Briolat, A., Falk, R., Simpson, D., Tuovinen, J.-P., Alonso, R., Barth, S., Baumgarten, M., Grulke, N., Karlsson, P.E., King, J., Lagergren, F., Matyssek, R., Nunn, A., Ogaya, R., Peñuelas, J., Rhea, L., Schaub,

M., Uddling, J., Werner, W. and Emberson, L.D.: DO3SE modelling of soil moisture to determine ozone flux to European forest trees, Atmos. Chem. Phys. 12, 5537–5562, 2012.

- Butterbach-Bahl K., Gasche R., Breuer L., and Papen H.: Fluxes of NO and $N_2O$ from temperate forest soils: impact of forest type, N deposition and of liming on the NO and $N_2O$ emissions, Nutr. Cycl. Agroecosyst. 48, 79-90, 1997.
- Campanaro A., Hardersen S., and Mason F.: Piano di Gestione della Riserva Naturale e Sito Natura 2000 "Bosco della Fontana". Quaderni Conservazione Habitat, 4. Cierre Edizioni, Verona (Italy), pp. 221, 2007,
- Cieslik S.: Energy and ozone fluxes in the atmospheric surface layer observed in Southern Germany highlands, Atmos. Environ., 32, 1273-1281, 1998
- Clifton O.E., Fiore A.M., Munger J.W., Malyshev S., Horowitz L.W., Shevliakova E., Paulot F., Murray L.T., Griffin K.L., 2016. Interannual variability in ozone removal by a temperate deciduous forest. *Geophys. Res. Let*., doi: 10.1002/2016GL070923.
- Coe, H., Gallagher, M. W., Choularton, T. W., and Dore, C.: Canopy Scale Measurements Of Stomatal And Cuticular O3 Uptake By Sitka Spruce, Atmos. Environ., 29, 1413–1423, 1995.
- Dalponte M., Giannelle D., and Bruzzone L.: Use of hyperspectral and LIDAR data for classification of complex forest areas. In: Gianelle D, Travaglini D, Mason F, Minari E, Chirici G, Chemini C (eds.) Canopy analysis and dynamics of a floodplain forest. Rapporti scientifici, 3, Cierre Grafica Editore, Verona, pp 25–37, 2007.
- Dorsey, J.R., Duyzer, J.H., Gallagher, M.W., Coe, H., Pilegaard, K., Weststrate, J.H.,Jensen, N.O., Walton, S.: Oxidized nitrogen and ozone interaction with forests. I: Experimental observations and analysis of exchange with Douglas fir, Q. J. Roy. Meteor. Soc., 130, 1941–1955, 2004.
- Emberson, L.D., Ashmore, M.R., Cambridge, H.M., Simpson, D., and Tuovinen, J.-P.: Modelling stomatal ozone flux across Europe, Environ. Pollut., 109, 3, 403-413, 2000.
- Ermel M., Oswald R., Mayer J.-C., Moravek A., Song G., Beck M., Meixner F. X., and Trebs I.: Preparation methods to optimize the performance of sensor discs for fast chemiluminescence ozone analyzers, Environ. Sci. Technol. 47, 1930-2936, 2013.
- Fares, S., Park, J.-H., Ormeno, E., Gentner, D. R., McKay, M., Loreto, F., Karlik, J., and Goldstein, A. H.: Ozone uptake by citrus trees exposed to a range of ozone concentrations, Atmos. Environ., 44, 3404–3412, doi:10.1016/j.atmosenv.2010.06.010, 2010.
- Fares, S., Weber, R., Park, J.-H., Gentner, D., Karlik, J., and Goldstein, A. H.: Ozone deposition to an orange orchard: Partitioning between stomatal and non-stomatal sinks, Environ. Pollut., 169, 258–266, doi:10.1016/j.envpol.2012.01.030, 2012
- Fares, S., F. Savi, A., Muller, J.B.A., Matteucci, G., Paoletti, E.: Simultaneous measurements of above and below canopy ozone fluxes help partitioning ozone deposition between its various sinks in a Mediterranean Oak Forest, Agr. Forest Meteorol. 198–199, 181–191, 2014.

- Finco, A., Marzuoli, R., Chiesa, M., and Gerosa. G.: Ozone risk assessment for an Alpine larch forest in two vegetative seasons with different approaches: comparison of POD1 and AOT40, Environ. Science and Poll. Res, 24 (34):26238-26248, 2017.
- Foken T. and Wichura B.: Tools for quality assessment of surface-based flux measurements, Agr. Forest Meteorol.,78, 83-205, 1996.
- Foken, T.: Micrometeorology, Springer-Verlag, Berlin Heidelberg, Germany, 2008.
- Foken, T., Meixner, F. X., Falge, E., Zetzsch, C., Serafimovich, A., Bargsten, A., Behrendt, T., Biermann, T., Breuninger, C., Dix, S., Gerken, T., Hunner, M., Lehmann-Pape, L., Hens, K., Jocher, G., Kesselmeier, J., Lüers, J., Mayer, J.-C., Moravek, A., Plake, D., Riederer, M., Rütz, F., Scheibe, M., Siebicke, L., Sörgel, M., Staudt, K., Trebs, I., Tsokankunku, A., Welling, M., Wolff, V., and Zhu, Z.: Coupling processes and exchange of energy and reactive and non-reactive trace gases at a forest site – results of the EGER experiment, Atmos. Chem. Phys., 12, 1923-1950, 2012.
- Fontan, J., Minga, A., Lopez, A. and Druilhet, A.: Vertical ozone profiles in a pine forest. Atmos. Environ. 26, 863–869, 1992.
- Fowler, D., Pilegaard, K., Sutton, M.A., Ambus, P., Raivonen, M., Duyzer, J., Simpson, D., Fagerli, H., Sandro Fuzzi, Schjoerring, J.K., Granier, C., Neftel, A., Isaksen, I.S.A., Laj, P., Maione, M., Monks, P.S., Burkhardt, J., Daemmgen, U., Neirynck, J., Personne, E., Wichink-Kruit, R., Butterbach-Bahl, K., Flechard, C., Tuovinen, J.P., Coyle, M., Gerosa, G., Loubet, B., Altimir, N., Gruenhage, L., Ammann, C., Cieslik, S., Paoletti, E., Mikkelsen, T.N., Ro-Poulsen, H., Cellier, P., Cape, J.N., Horváth, L., Loreto, F., Niinemets, U., Palmer, P.I., Rinne, J., Misztal, P., Nemitz, E., Nilsson, D., Pryor, S., Gallagher, M.W., Vesala, T., Skiba, U., Brüggemann, N., Zechmeister-Boltenstern, S., Williams, J., O'Dowd, C., M.C. Facchini, de Leeuw, G., Flossman, A., Chaumerliac, N., and Erisman, J.W.: Atmospheric Composition Change: Ecosystems – Atmosphere interactions, Atmos. Environ., 43, 5193-5267, 2009.
- Fuentes, J. D., Gillespie, T. J., Denhartog, G., and Neumann, H. H.: Ozone Deposition onto a Deciduous Forest During Dry and Wet Conditions, Agr. Forest Meteorol., 62, 1–18, 1992.
- Gasche R., and Papen H.: A 3-year continuous record of nitrogen trace gas fluxes from untreated and limed soil of a N-saturated spruce and beech forest ecosystem in Germany. 2. NO and $NO_2$ fluxes, J. Geophys. Res. 104, 18505-28520, 1999.
- Gerosa, G., Fusaro, L., Monga, R., Finco, A., Fares, S., Manes, F. and Marzuoli, R.:. A flux-based assessment of above and below ground biomass of Holm oak (*Quercus ilex* L.) seedlings after one season of exposure to high ozone concentrations, Atmospheric Environment 113, 41-49, 2015.
- Gerosa G., M,arzuoli, R., Monteleone, B., Chiesa, M. and Finco, A.: Vertical ozone gradients above forests. Comparison of different calculation options with direct ozone measurements above a mature forest and consequences for ozone risk assessment, Forests, 8, 337, 2017.

- Gerosa, G., Vitale, M., Finco, A., Manes, F., Ballarin-Denti, A., and Cieslik, S.: Ozone uptake by an evergreen Mediterranean forest (Quercus ilex) in Italy. Part I: micrometeorological flux measurements and flux partitioning, Atmos. Environ. 39, 3255-3266, 2005.
- Gerosa, G., Finco, A., Mereu, S., Vitale, M., Manes, F., Ballarin-Denti, A.: Comparison of seasonal variations of ozone exposure and fluxes in a Mediterranean Holm oak forest between the exceptionally dry 2003 and the following year, Environ. Pollut. 157, 1737–1744, 2009a.
- Gerosa, G., Finco, A., Mereu, S., Marzuoli, R., and Ballarin-Denti, A.: Interactions among vegetation and ozone, water and nitrogen fluxes in a coastal Mediterranean maquis ecosystem, Biogeosciences 6, 1783-1798, 2009b.
- Goldstein, A. H., McKay, M., Kurpius, M. R., Schade, G. W., Lee, A., Holzinger, R., and Rasmussen, R. A.: Forest thinning experiment confirms ozone deposition to forest canopy is dominated by reaction with biogenic VOCs, Geophys. Res. Lett., 31, L22106, doi: 10.1029/2004GL21259, 2004.
- Güsten H., and Heinrich G.: On-line measurements of ozone surface fluxes: Part I. Methodology and instrumentation, Atmos. Environ. 6, 897-909, 1996.
- Jarvis P.G.: The interpretation of the variations in leaf water potential and stomatal conductance found in canopies in the field, Philos. T. Roy. Soc. B., 273, 593–610, 1976.
- Keronen, P., Reissell, A., Rannik, U., Pohja, T., Siivola, E., Hiltunen, V., Hari, P., Kulmala, M., and Vesala, T.: Ozone flux measurements over a Scots pine forest using eddy covariance 25 method: performance evaluation and comparison with flux-profile method, Boreal Environ. Res., 8, 425–444, 2003.
- Lamaud, E., Carrara, A., Brunet, Y., Lopez, A., and Druilhet, A.: Ozone fluxes above and within a pine forest canopy in dry and wet conditions, Atmos. Environ., 36, 77–88, 2002.
- Langford, B., Acton, W., Ammann, C., Valach, A., and Nemitz, E.: Eddy-covariance data with low signal-to-noise ratio: time-lag determination, uncertainties and limit of detection, Atmos. Meas. Tech. 8, 4197-4213, 2015.
- Launiainen, S., Katul, G.G., Gronholm, T., and Vesala, T.: Partitioning ozone fluxes between canopy and forest floor by measurements and a multi-layer model, Agr. Forest Meteorol. 173, 85–99, 2013.
- Lee X., Massman W., and Law B.: Handbook of Micrometeorology: A Guide for Surface Flux Measurements and Analysis, Kluwer Academic Publisher, Dordrecht, 2004.
- Longo L.: Clima. In: Mason F. (ed.). Dinamica di una foresta della Pianura Padana. Bosco della Fontana. Seconda edizione con Linee di gestione forestale. Rapporti Scientifici 1. Centro Nazionale Biodiversità Forestale Verona - Bosco della Fontana. Arcari Editore, Mantova (Italy), pp. 16-27, 2004.
- Marzuoli, R., Bussotti, F., Calatayud, V., Calvo, E., Alonso, R., Bermejo, V., Pollastrini, M., Monga, R. and Gerosa, G.: Dose-response relationships for ozone effect on the growth of deciduous broadleaf oaks in mediterranean environment, Atmos. Env., 190, 331-341.

- Matyssek, R., Wieser, G., Calfapietra, C., de Vries, W., Dizengremel, P., Ernst, D., Jolivet, Y., Mikkelsen, T.T., Mohren, G.M.J., Le Thiec, D., Tuovinen, J.P., Weatherall, A., and Paoletti, E.: Forests under climate change and air pollution: gaps in understanding and future directions for research, Environ. Pollut. 160, 57–65, 2012.
- McMillen, R.T.: An Eddy Correlation Technique with Extended Applicability to Non-Simple Terrain, Boundary-Lay Meteorol. 43, 231–245, 1988.
- Mikkelsen, T. N., Ro-Poulsen, H., Hovmand, M. F., Jensen, N.O., Pilegaard, K. and Egeløv, A. H.: Five-year measurements of ozone fluxes to a Danish Norway spruce canopy, Atmos. Environ. 38, 2361-2371, 2004.
- Muller, J. B. A., Percival, C. J., Gallagher, M. W., Fowler, D., Coyle, M. and Nemitz, E.: Sources of uncertainty in eddy covariance ozone flux measurements made by dry chemiluminescence fast response analysers, Atmos. Meas. Tech., 3, 163-176, 2010.
- Padro J.: Summary of ozone dry deposition velocity measurements and model estimates over vineyard, cotton, grass and deciduous forest in summer, Atmos. Environ., 30, 2363-2369, 1996.
- Pilegaard, K.: Air–soil exchange of NO, $NO_2$ and $O_3$ in forests, Water, Air, and Soil Poll.: Focus 1, 79–88, 2001.
- Rannik, Ü., Altimir, N., Mammarella, I., Bäck, J., Rinne, J., Ruuskanen, T. M., Hari, P., Vesala, T., and Kulmala, M.: Ozone deposition into a boreal forest over a decade of observations: evaluating deposition partitioning and driving variables, Atmos. Chem. Phys., 12, 12165-22182, https://doi.org/10.5194/acp-22-22165-2012, 2012.
- Rosenkranz, P., Brüggemann, N., Papen, H., Xu, Z., Seufert, G., and Butterbach-Bahl, K.: $N_2O$, NO and $CH_4$ exchange, and microbial N turnover over a Mediterranean pine forest soil, Biogeosciences 3, 121-133, 2006.
- Rummel, U., Ammann, C., Gut, A., Meixner, F. X., and Andreae, M. O.,. Eddy covariance measurements of nitric oxide flux within an Amazonian rainforest, J. Geophys. Res. Atm.: 107, D20, 17, 1-9, 2002.
- Rummel, U., Ammann, C., Kirkman, G. A., Moura, M. A. L., Foken, T., Andreae, M. O., and Meixner, F. X.: Seasonal variation of ozone deposition to a tropical rain forest in southwest Amazonia, Atmos. Chem. Phys. 7, 5415–5435, 2007.
- Schallhart, S., Rantala, P., Nemitz, E., Taipale, D., Tillmann, R., Mentel, T. F., Loubet, B., Gerosa, G., Finco, A., Rinne, J., and Ruuskanen, T. M.: Characterization of total ecosystem-scale biogenic VOC exchange at a Mediterranean oak–hornbeam forest, Atmos. Chem. Phys. 16, 7171-7194, 2016.
- Schotanus, P., Nieuwstadt, F., and De Bruin, H. A. R.: Temperature measurement with a sonic anemometer and its application to heat and moisture fluxes, Boundary-Lay. Meteorol.26, 81-93, 1983.
- Stella, P., Loubet, B., Lamaud, E., Laville, P., and Cellier, P.: Ozone deposition onto bare soil: a new parameterisation, Agr. Forest Meteorol., 151, 669–681, 2011.
- Stella, P., Kortner, M., Ammann, C., Foken, T., Meixner, F. X., and Trebs, I.: Measurements of nitrogen oxides and ozone fluxes by eddy covariance at a meadow: evidence for an internal leaf resistance to NO2, Biogeosciences, 10, 5997-6017, 2013.

- Teklemariam, T. A. and Sparks, J. P.: Leaf fluxes of NO and NO2 in four herbaceous plant species: The role of ascorbic acid, Atmos. Environ., 40, 2235-2244, 2006.
- Utiyama, M., Fukuyama, T., Maruo, Y.Y., Ichino, T., Izumi, K., Hara, H., Takano, K.,Suzuki, H., Aoki, M.: Formation and deposition of ozone in a red pine forest. Water, air, and soil poll. 151, 53–70. 2004
- Vickers D. and Mahrt L.: Quality Control and Flux Sampling Problems for Tower and Aircraft Data, J. Atmos. Oceanic Technol., 14, 512–526, 1997.
- Webb, E. K., Pearman, G. I., and Leuning, R.: Correction of flux measurements for density effects due to heat and water vapour transfer, Q. J. Roy. Meteor. Soc. 106, 85–100, 1980.
- Wilczak J. M., Oncley S. P., Sage,S. A.: Sonic anemometer tilt correction algorithms, Boundary-Lay. Meteorol. 99, 127-150, 2001.
- Wittig, V.E., Ainsworth, E.A., Naidu, S.L., Karnosky, D.F., Long, S.P., 2009. Quantifying the impact of current and future tropospheric ozone on tree biomass, growth, physiology and biochemistry: a quantitative meta-analysis, Global Change Biol. 15, 396–424.
- Wu X., Brüggemann N., Gasche R., Shen Z., Wolf B., and Butterbach-Bahl K.: Environmental controls over soil-atmosphere exchange of $N_2O$, NO, and $CO_2$ in a temperate Norway spruce forest, Global Biogeochem. Cy. 24, 2, 2010.
- Zona, D., Gioli, B., Fares, S., De Groote, T., Pilegaard, K., Ibrom, A., and Ceulemans, T.: Environmental controls on ozone fluxes in a poplar plantation in Western Europe, Environ. Pollut., 184, 201-210, 2014.

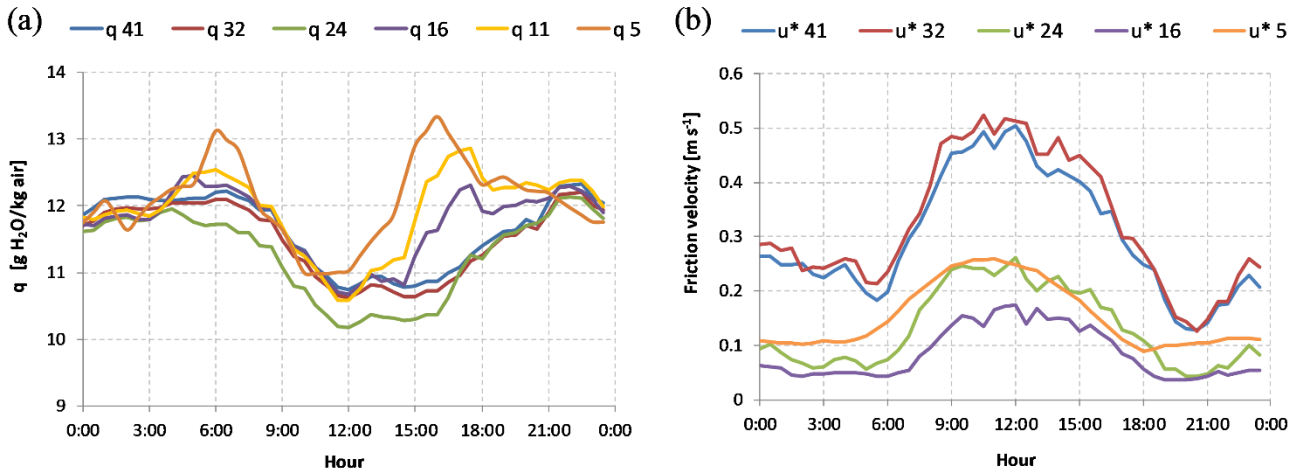


**Figure 1 – (a) Average diel course of specific humidity at the five levels; (b) Average diel course of friction velocity at the five heights. For both figures the numbers in the curves label of the legend represent the measurement height (in meters). For figure (a) the maximum and the minimum standard error of the half-hourly means were respectively 0.45 g and 0.24 g $H_2O$/kg air for 41 m, 0.45 g and 0.25 g for 32 m, 0.49 and 0.24g $H_2O$/kg air for 24 m, 0.49 and 0.24 g $H_2O$/kg air for 16 m, 0.52 and 0.25g $H_2O$/kg air for 5 m. For figure (b) The maximum and the minimum standard error of the half-hourly means were respectively 0.05 and 0.02 m $s^{-1}$ for 41 m, 0.06 and 0.03 m $s^{-1}$ for 32 m, 0.03 and 0.01 m $s^{-1}$ for 24 m, 0.02 and 0.01 m $s^{-1}$ for 16 m, 0.02 and 0.01 m $s^{-1}$ for 5 m.**

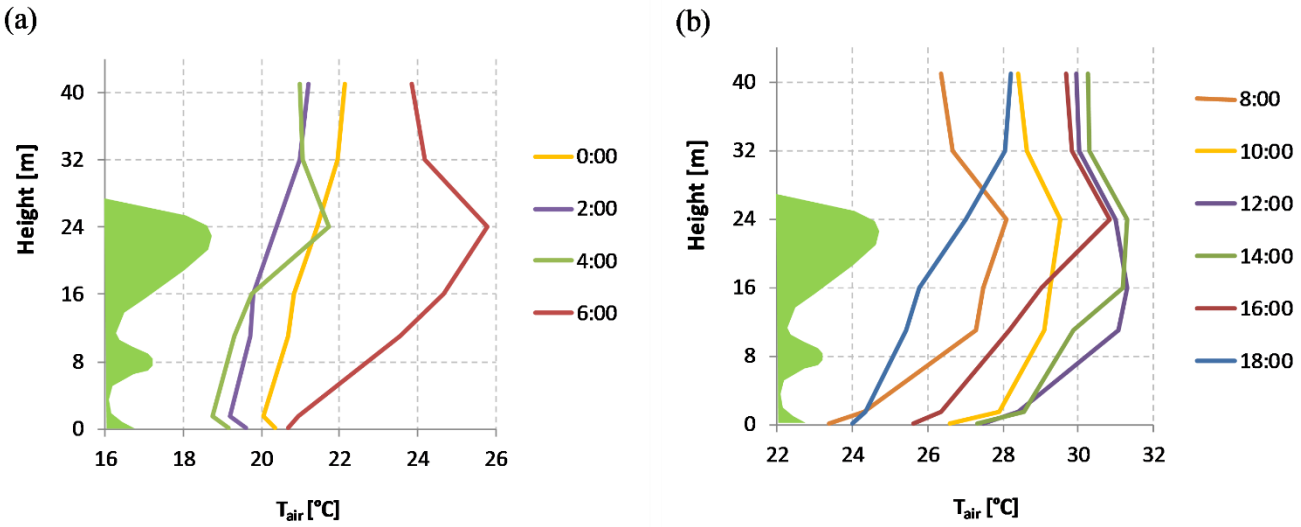


**Figure 2 - Diurnal evolution of vertical profile of air temperature. (a) from 0:00 to 6:00 AM; (b) from 8:00 to 18:00. The green shaded area represents the vertical distribution of vegetation. The maximum and the minimum standard error of the half-hourly means were respectively, 0.35 and 0.32 °C for 0:00, 0.38 and 0.36 °C for 2:00, 0.40 and 0.37 °C for 4:00, 0.42 and 0.35 °C for 6:00, 0.35 and 0.31 °C for 8:00, 0.39 and 0.33 °C for 10:00 m, 0.40 and 0.33 °C for 12:00, 0.70 and 0.62 °C for 14:00, 0.73 and 0.52 °C for 16:00, 0.54 and 0.40 °C for 18:00.**

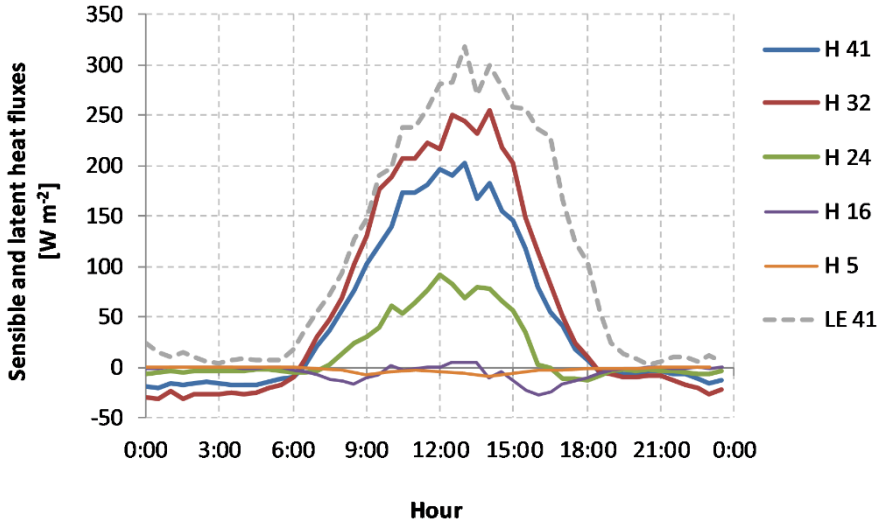


**Figure 3 - Average diel course of sensible heat fluxes at the five levels (41 m, 32 m, 24 m, 16 m and 5 m, thick lines) and latent heat flux measured at 41 m (dashed line). The maximum and the minimum standard error of the half-hourly means for sensible heat fluxes were respectively 20.3 and 1.1 W $m^{-2}$ for 41 m, 27.1 and 2.0 W $m^{-2}$ for 32 m, 9.2 and 1.0 W $m^{-2}$ for 24 m, 4.3 and 0.3 W $m^{-2}$ for 16 m, 3.7 and 0.4 W $m^{-2}$ for 5 m, 28.7 and 1.4 W $m^{-2}$ for latent heat fluxes at 41 m.**

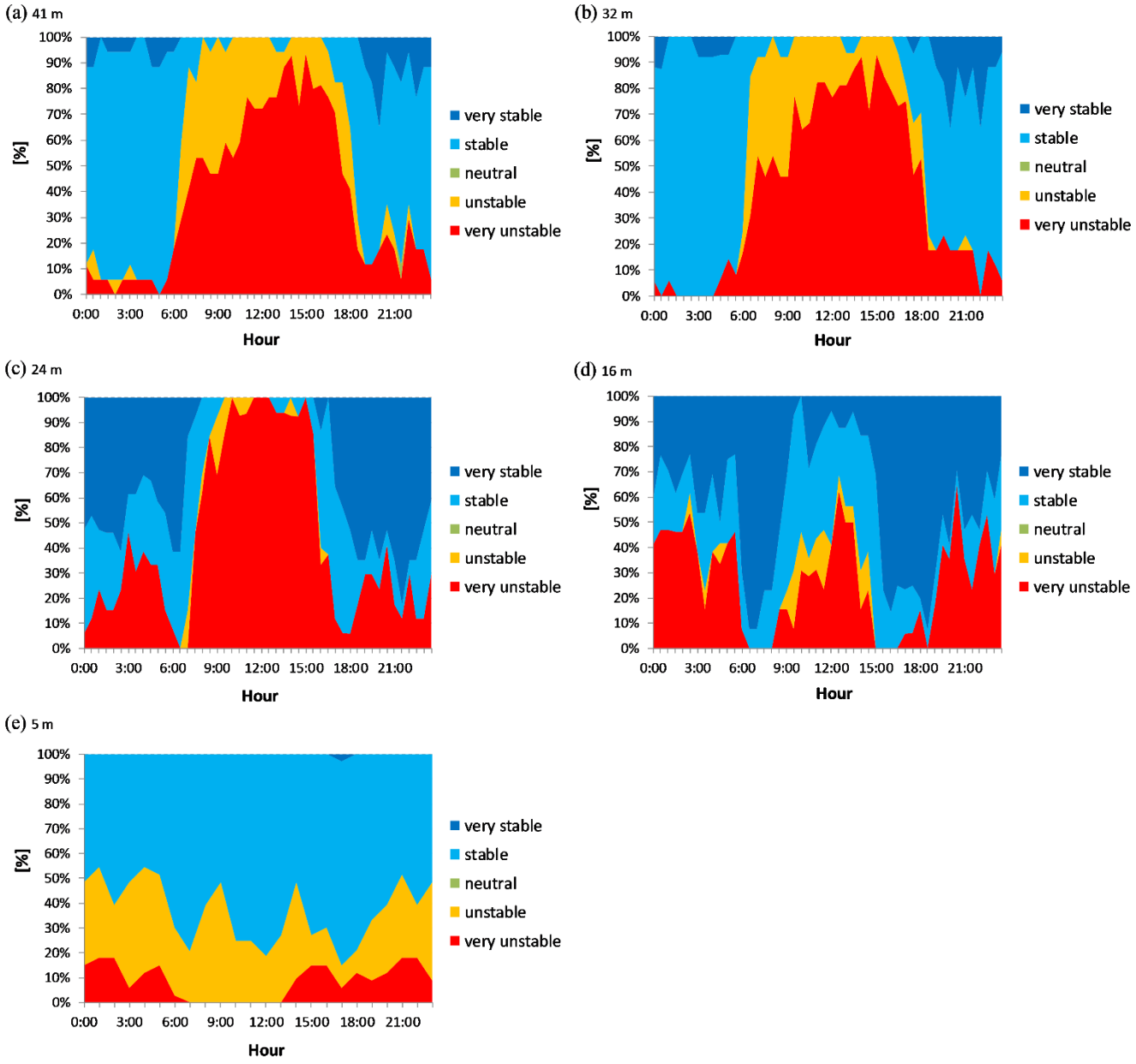


**Figure 4 - Stability class distributions in the different hours of the day expressed as function of z/L for the different levels: (a) 41 m, (b) 32 m, (c) 24 m and (d) 16 m (e) 5 m. z is the measuring height while L is the Obhukov length. The stability classes were classified as follows according to Gerosa et al. (2017): very stable: 0<L≤10; stable: 10<L≤100'000; neutral: abs(L)>100'000; unstable: -100'000≤L<100; very unstable: -100≤L<0.**

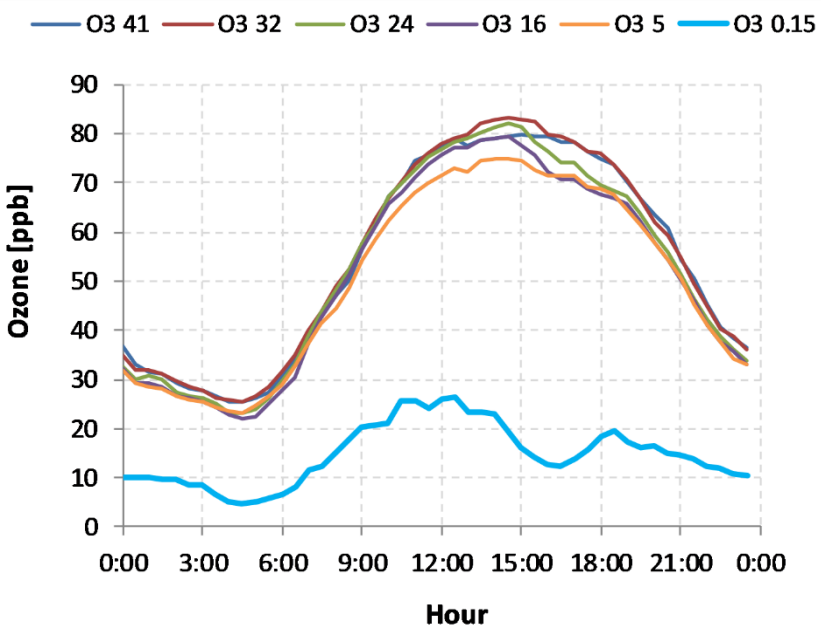


**Figure 5 - Average diel courses of ozone concentrations at six levels (41 m, 32 m, 24 m, 16 m, 5 m and 0.15 m). The maximum and the minimum standard error of the half-hourly means were respectively 3.0 and 1.7 ppb for 41 m, 3.0 ppb 1.8 ppb for 32 m, 3.4 and 1.9 ppb for 24 m, 3.4 and ppb 1.8 for 16 m, 2.9 and 1.7 ppb for 5 m, 3.4 ppb and 1.0 ppb for 0.15 m.**

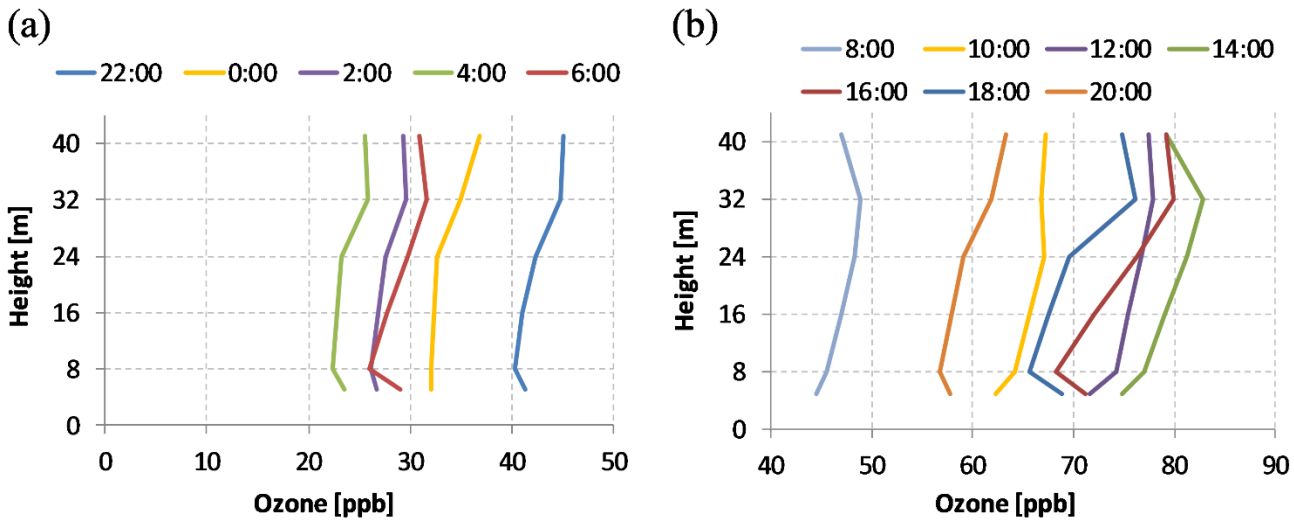


**Figure 6 - Diurnal evolution of ozone concentration profiles: (a) from 22:00 to 6:00; (b) from 8:00 to 20:00. The time of the day to which measurements are referred is indicated in each figure label. The 0.15 m level has not been included here for a better visualization (ozone concentration at this level was around 10 ppb in (a) and below 25 ppb in (b)). The maximum and the minimum standard error of the half-hourly means were respectively 2.9 and 2.5 ppb for 0:00, 2.3 and 2.0 ppb for 2:00, 2.7 and 2.5 ppb for 4:00, 2.9 and 2.5 ppb for 6:00, 2.3 and 2.0 ppb for 8:00, 2.1 and 1.9 ppb for 10:00, 1.9 and 1.7 ppb for 12:00, 2.4 and 1.9 ppb for 14:00, 2.7 and 2.2 ppb for 16:00, 2.9 and 2.4 ppb for 18:00, 2.6 and 2.1 ppb for 20:00, 2.5 ppb and 1.9 ppb for 22:00.**

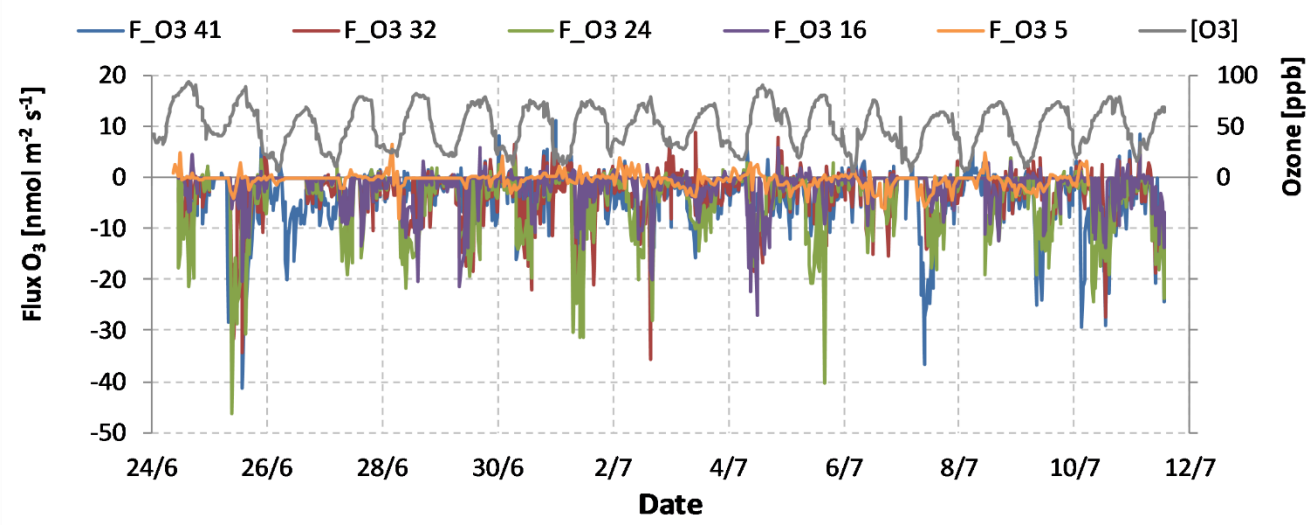


**Figure 7 - Ozone fluxes at the five levels (41 m, 32 m, 24 m, 16 m and 5 m) and ozone concentration at 41 m during the "Flux Profile period".**

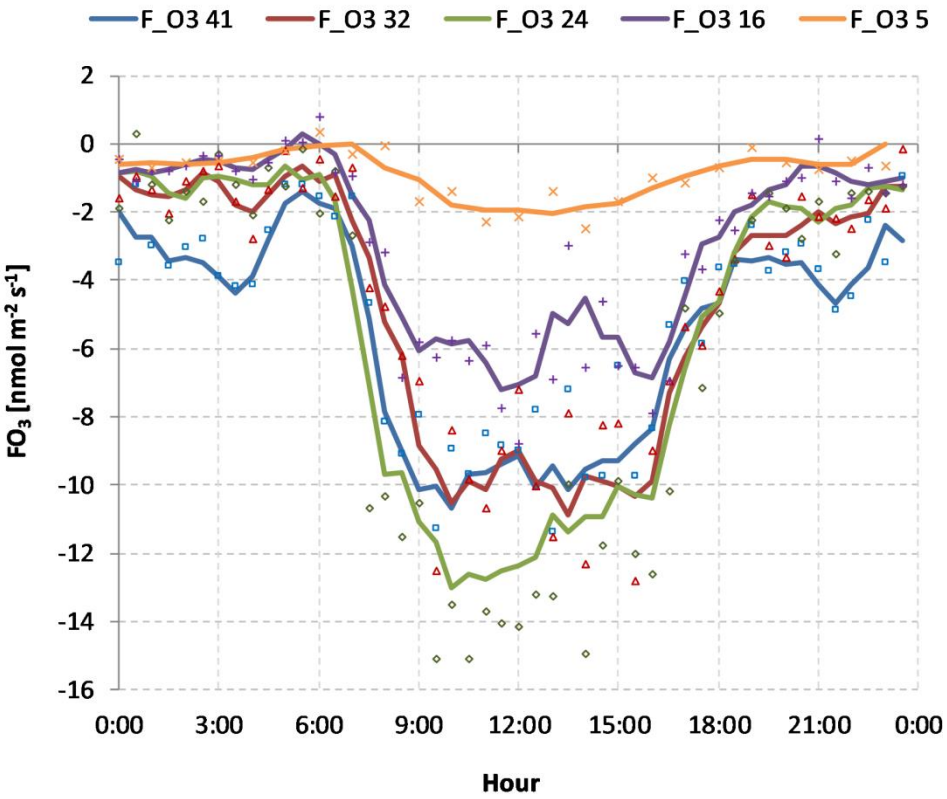


**Figure 8 - Average diel courses of ozone fluxes during the "Flux Profile period" at the five levels (41 m, 32 m, 24 m, 16 m and 5 m). Dots represent half-hourly averages while lines are one hour and half running means centered on each half-hour. The maximum and the minimum standard error of the half-hourly means of $O_3$ fluxes were respectively 2.9 and 0.7 nmol $m^{-2}$ $s^{-1}$ for 41 m, 2.6 and 0.4 nmol $m^{-2}$ $s^{-1}$ for 32 m, 2.7 and 0.2 nmol $m^{-2}$ $s^{-1}$ for 24 m, 2.1 and 0.2 nmol $m^{-2}$ $s^{-1}$ for 16 m, 0.7 and 0.1 nmol $m^{-2}$ $s^{-1}$ for 5 m.**

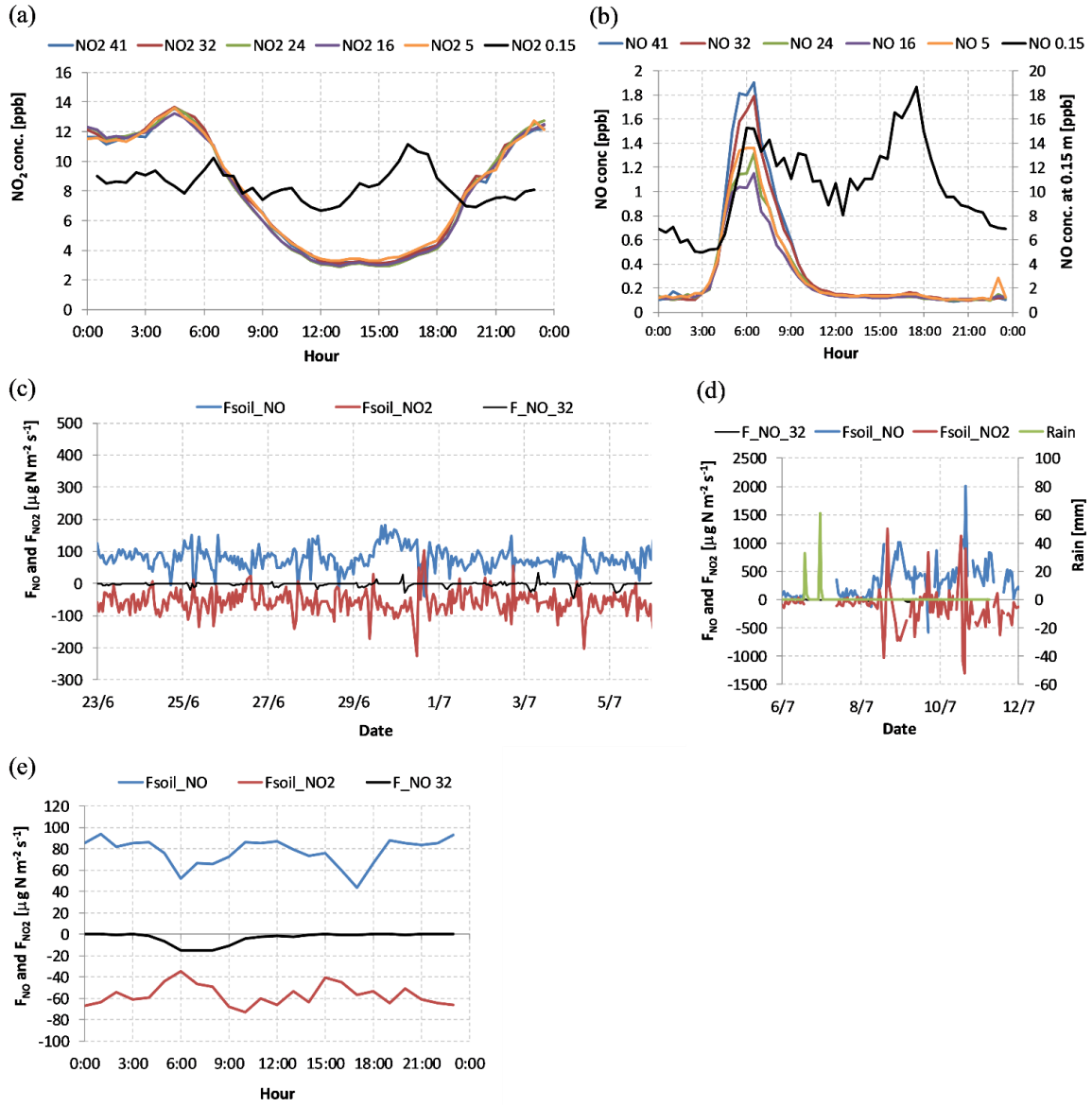


**Figure 9 - NO and $NO_2$ concentrations and fluxes during the "Flux Profile period". (a) Average diel course of NO concentrations at the five levels (41 m, 32 m, 24 m, 16 m and 5 m); (b) Average diel course of $NO_2$ concentrations; c) Soil NO and $NO_2$ fluxes and NO fluxes at 32 m before rainfalls events; (d) Soil NO and $NO_2$ fluxes and NO fluxes at 32 m after rainfall events (green line); (e) Average diel course of soil NO and $NO_2$ fluxes and of NO fluxes at 32 m. Please, note the different scale between (c) and (d). For figure (a), the maximum and the minimum standard error of the half-hourly means of $NO_2$ were respectively 1.74 and 0.14 ppb for 41 m, 1.71 and 0.12 ppb for 32 m, 1.71 and 0.12 ppb for 24 m, 1.55 and 0.15 ppb for 16 m, 1.55 and 0.17 ppb for 5 m, 2.12 and 0.57 ppb for 0.15 m. For figure (b), the maximum and the minimum standard error of the half-hourly means of NO were respectively 0.45 and 0.006 ppb for 41 m, 0.41 and 0.003 ppb for 32 m, 0.41 and 0.004 ppb for 24 m, 0.34 and 0.004 ppb for 16 m, 0.34 and 0.004 ppb for 5 m, 3.11 and 0.65 ppb for 0.15 m. For figure (e) the maximum and the minimum standard error of the half-hourly means were respectively 11.0 and 3.6 µg N $m^{-2}$ $s^{-1}$ for F_NO soil, 16.2 and 4.2 µg N $m^{-2}$ $s^{-1}$ for F_$NO_2$ soil, 4.3 and 0.1 µg N $m^{-2}$ $s^{-1}$ for F_NO 32.**

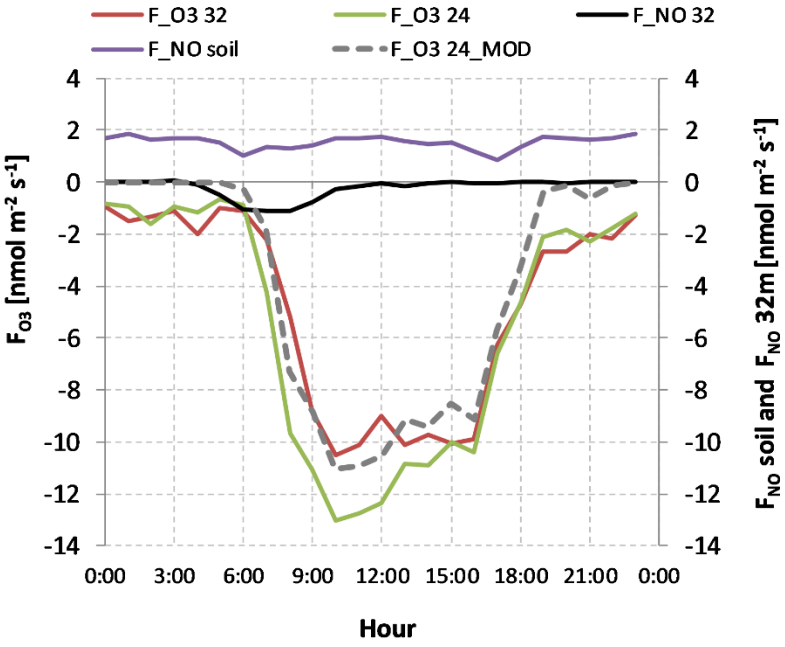


**Figure 10 - Average diel course of ozone fluxes at 32 m (red line), ozone fluxes at 24 m (green line), NO fluxes at 32 m (black line) soil NO fluxes (purple line) and modified ozone fluxes at 24 m (dashed grey line). This latter takes into account the role of the NO sink.**

5

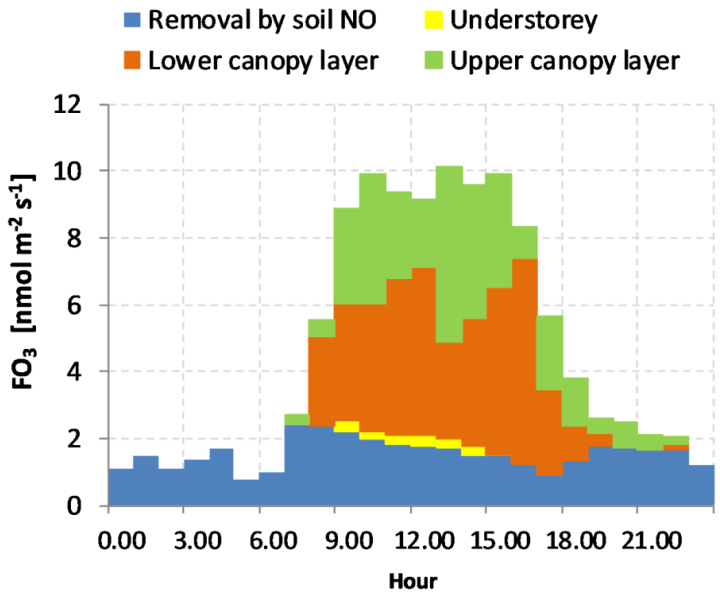


**Figure 11 - Average diel course of the ozone removal by the different forest layers and by the NO emitted from the forest floor.**

5

# Supplementary material

**Table S1 - Instruments installed at each level of the tower and on the mast at 5 m a.g.l. In brackets are indicated the variable measured by each instrument and the manufacturer. (T is air temperature, RH is relative humidity, NR is net radiation, P is pressure, Rain is precipitation, SWC is soil water content, SHF is soil heat flux). The Soil dynamic chamber system is described in the methodological part.**

| Level / Height (m) | Ultrasonic anemometer | Fast ozone analyzer | Other fast analyzer | Slow sensors | |
|---|---|---|---|---|---|
| **41** | USA1 (*Metek, D*) | COFA (*Ecometrics, I*) | LI-COR 7500 ($CO_2$, $H_2O$, *Li-Cor, USA*) | HMP45<br>NR-lite<br>BF5<br>PTB101B<br>Rain gauge 52202 | (T, RH, *Vaisala, FIN*)<br>(NR, *Kipp & Zonen, NL*)<br>(PAR,*Delta-T Devices, UK*)<br>(P, *Vaisala, FIN*)<br>(Rain, *Campbell Scientific, USA*) |
| **32** | HS50 (*Gill, UK*) | ROFI (*CEH, UK*) | CLD780TR (NO, *Ecophysics, CH*) | HMP45 | (T, RH, *Vaisala, FIN*) |
| **24** | Windmaster PRO (*Gill, UK*) | FROM (*NOAA, USA*) | - | HMP45 | (T, RH, *Vaisala, FIN*) |
| **16** | Windmaster PRO (*Gill, UK*) | COFA (*Ecometrics, I*) | - | HMP45 | (T, RH, *Vaisala, FIN*) |
| **11** | - | - | - | HMP45 | (T, RH, *Vaisala, FIN*) |
| **5** | R2 (*Gill, UK*) | FOS (*Sextant, NZ*) | LI-COR 7500 ($CO_2$, *Li-Cor, USA*) | | - |
| **1.5** | - | - | - | PT100 | (T, *Campbell Scientific, USA*) |
| **0.15** | - | - | - | PT100 | (T, *Campbell Scientific, USA*) |
| **Soil** | - | - | - | TDR mod 616<br>HFP01SC<br>PT100<br>Soil dynamic chamber system (*IMK-IFU, D*) | (SWC, *Campbell Scientific, USA*)<br>(SHF, *Hukseflux, NL*)<br>(T, *GMR Strumenti, I*) |

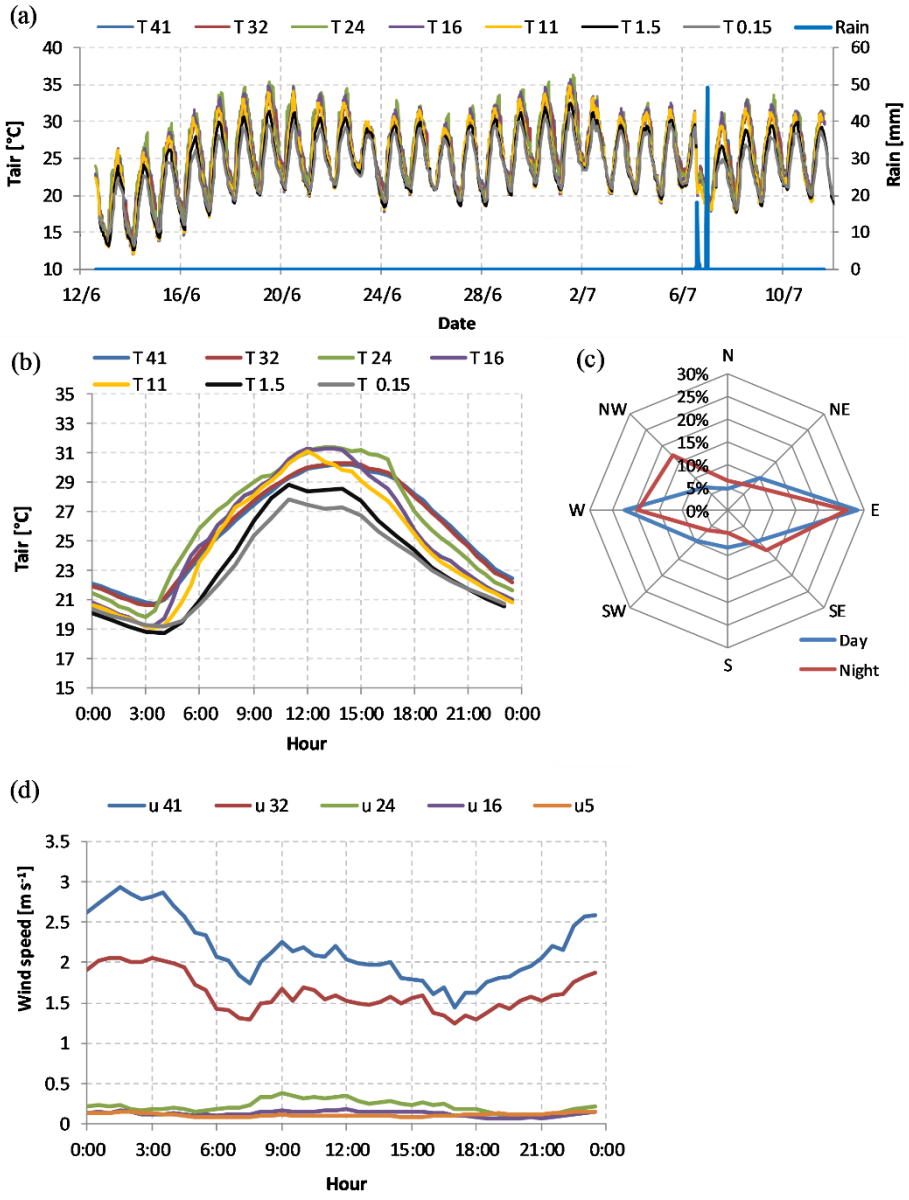


**Figure S1 – (a) Rainfall amounts and temperature evolution at the seven heights. Blue lines are rainfalls. (b) Average diel course of air temperature at the seven heights. (c) Wind rose based on 41 m data, the radial axis unit indicates the percentage of the data in each direction, the blue line diurnal data, the red line nighttime data. (d) Average diel course of wind intensity at the five heights. For figures a), b), d) and e) the numbers in the curves label of the legend represent the measurement height (in meters). For figure b) The maximum and the minimum standard error of the half-hourly means were respectively 0.65 and 0.32 °C for 41 m, 0.66 and 0.33 °C for 32 m, 0.73 and 0.33 for 24 m, 0.71 and 0.31 °C for 16 m, 0.68 and 0.30 °C for 11 m, 1.10 and 0.65 °C for 1.5 m, 1.11 and 0.66 °C for 0.15 m. For figure (d) The maximum and the minimum standard error of the half-hourly means were respectively 0.32 and 0.12 m $s^{-1}$ for 41 m, 0.28 and 0.08 m $s^{-1}$ for 32 m, 0.05 and 0.01 m $s^{-1}$ for 24 m, 0.02 and m $s^{-1}$ 0.01 for 16 m, 1.11 and 0.03 m $s^{-1}$ for 5 m.**

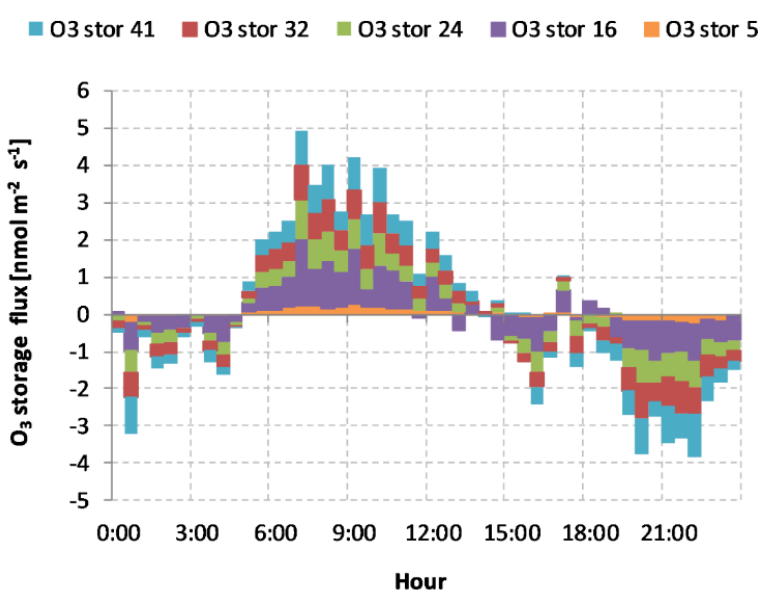


**Figure S2 - Mean diel evolution of the ozone storage flux (the storage term of the Eq. 3). The contribution of the air column between adjacent flux measurement levels is indicated with a different color.**

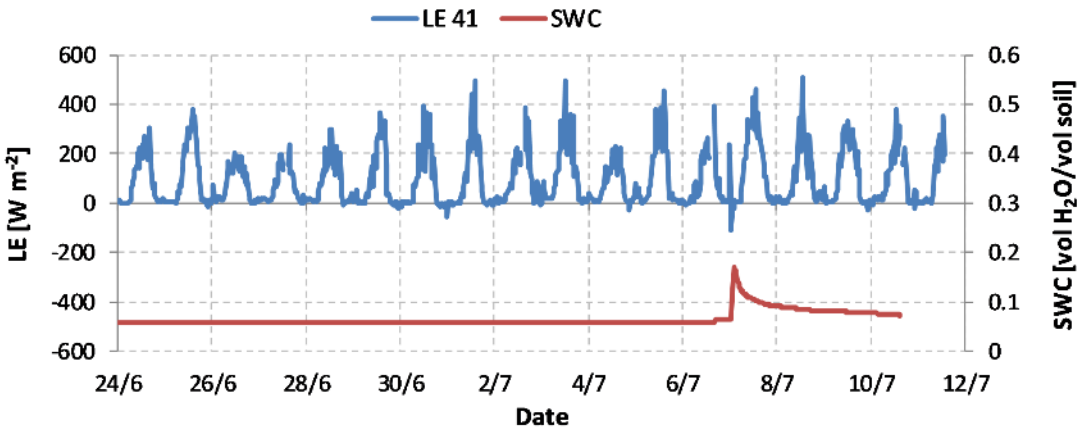


**Figure S3 - Latent heat fluxes measured at the top of the tower (LE 41) and soil water content (SWC) expressed as volumetric ratio between water and soil.**

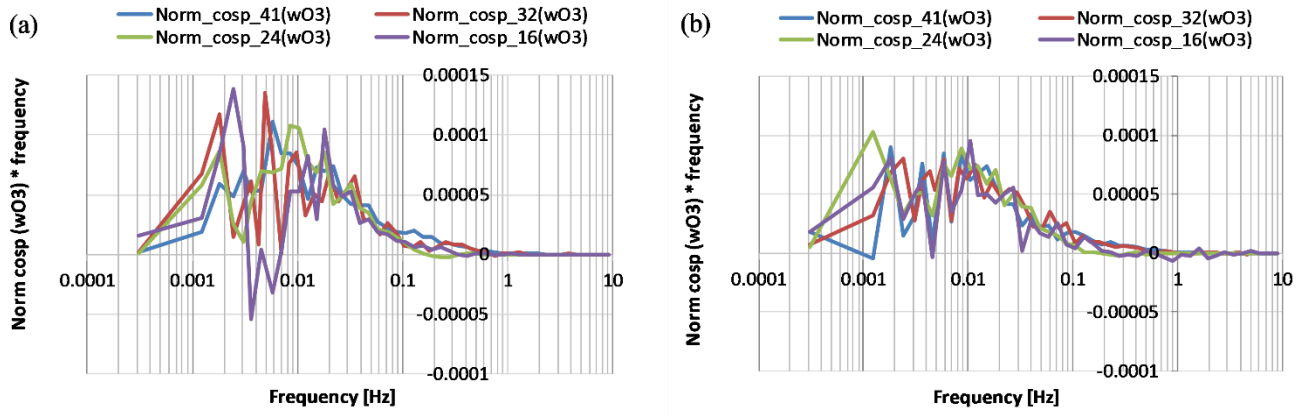


**Figure S4 - Average normalized cospectra of the vertical component of the wind and ozone at 11:00 (a) and at 15:00 (b).**

5